Mutations in SARS-CoV-2 Variants Modulate the Microscopic Dynamics of Neutralizing Antibodies

Dhiman Ray,[†] Riley Nicolas Quijano,[†] and Ioan Andricioaei[*,‡,‡]

†*Department of Chemistry, University of California Irvine, Irvine CA 92697*

‡*Department of Physics and Astronomy, University of California Irvine, Irvine CA 92697*

E-mail: andricio@uci.edu

Abstract

Monoclonal antibodies have emerged as viable treatment for the COVID-19 disease caused by the SARS-CoV-2 virus. But the new viral variants can reduce the efficacy of the currently available antibodies, as well as diminish the vaccine induced immunity. Here, we demonstrate how the microscopic dynamics of the SARS-CoV-2 neutralizing monoclonal antibodies, can be modulated by the mutations present in the spike proteins of the variants currently circulating in the world population. We show that the dynamical perturbation in the antibody structure can be diverse, depending both on the nature of the antibody and on the location of the mutation. The correlated motion between the antibody and the receptor binding domain (RBD) can also be changed, altering the binding affinity. By constructing a protein graph connectivity network, we could delineate the mutant induced modifications in the allosteric information flow pathway through the antibody, and observed the presence of both localized and long distance effects. We identified a loop consisting of residues 470-490 in the RBD which works like an anchor preventing the detachment of the antibodies, and individual mutations in that region can significantly affect the antibody binding propensity. Our study provides fundamental and atomistically detailed insight on how virus neutralization by monoclonal antibody can be impacted by the mutations in the epitope, and can potentially facilitate the rational design of monoclonal antibodies, effective against the new variants of the novel coronavirus.

Introduction

The coronavirus disease 19 (COVID-19) caused by the severe acute respiratory syndrome coronavirus 2 (SARS-CoV-2)[1] has claimed more than 4 million lives worldwide, as of July 2021, creating a global pandemic and one of the largest public health crises in human history.[2] To address this urgent problem, scientists across various disciplines have engaged in active collaboration to develop therapeutic agents like drugs, vaccines, and antibodies against this deadly virus.[3–7] The spike proteins, present on the surface of the virus, recognize and bind

to the human angiotensin converting enzyme 2 (hACE2) receptor in the lung cells to initiate the infection.[8,9] The receptor binding domain (RBD) of the spike is a key target for drug development and antibody recognition.[10–16] A large fraction of monoclonal antibodies (mAb), and the antibodies (Ab) generated by the immune system, blocks the infection by binding to the RBD and preventing it to attach with the hACE2 receptor. Moreover, many of the currently available vaccines, such as the ones developed by Pfizer,[17] Moderna,[18] and AstraZeneca,[19] use the spike protein as their epitope and induce immunity by generating antibodies and memory cells that can potentially recognize regions of the spike protein including the RBD.

The process of antigen-antibody recognition is of fundamental importance for developing immune response against pathogens invading our body. Since their discovery in 1975, monoclonal antibodies (mAb) found a wide range of therapeutic applications, particularly in the treatment of cancer, chronic inflammation and infectious diseases caused by virus.[20] Monoclonal antibodies, engineered in laboratory, have identical protein sequence, facilitating their use for treating specific diseases. They are generated by identical B-lympocyte immune cells cloned from a unique parent white blood cell. The use of engineered antibodies as drugs has become increasingly appealing due to their high binding affinity and antigen specificity determined by their complementarity determining regions (CDR) within variable heavy (V_H) and variable light (V_L) chains.[21]

Monoclonal antibodies have significant advantages over conventional passive immunization techniques like convalescent plasma therapy (CPT), by reducing the risk of blood-borne diseases, shortening the time needed to generate high affinity and low risk antibodies, and allowing for variable epitope specificity.[22] A number of monoclonal antibodies have been reported to neutralize the novel coronavirus and are at various stages of clinical trial, with Bamlanivimab and REGN-COV2 receiving emergency use authorization (EUA) in the United States of America by the Food and Drug Administration (FDA) as of June 2021.[23] Molecular structures of multiple monoclonal antibodies, in complex with spike protein of

SARS-CoV-2, have been resolved, facilitating detailed structural studies to understand the antigen recognition process.[24–31]

The major concern for these treatments is the possibility of the appearance of new variants, with mutations in the RBD region, which can evade the immune response and reduce or nullify the action of neutralizing antibodies. Multiple such variants of SARS-CoV-2 have emerged throughout the course of the pandemic, threatening the effectiveness of current therapeutics against coronavirus. One of the earliest well documented variant, with mutations in RBD, was the B.1.1.7 strain, a.k.a. the *alpha* variant. It appeared in the United Kingdom in the latter half of 2020 and spread across the entire world due to its 70-80% higher transmissibility compared to the wild type.[32] This variant contains a N501Y mutation in the RBD, which has been attributed to its increased immune evasion capability, although no significant increase in reinfection was observed.[33] The next major highly infectious variant is the *beta* variant or the B.1.351 strain, originating in South Africa in October 2020. Apart from the N501Y, it has two more mutations in the RBD: K417N and E484K, and has been shown to reduce the effectiveness of conventional antibody therapy up to 10-fold.[34] Later, a new strain (B.1.617) with two RBD mutations, L452R and E484Q, emerged in India, and became officially known as the *kappa* variant. A lineage of that strain, B.1.617.2, is named as the *delta* variant by the World Health Organization (WHO). With 50-67% higher infectivity than the *alpha* strain,[35] the *delta* variant is designated as a *variant of concern* (along with *alpha* and *beta*) due to its potential to make currently available vaccines less effective in preventing serious illness.

To address this urgent crisis, a number of computational studies have been performed to obtain a molecular level understanding about how mutations in the RBD affect its binding with the hACE2 receptor and antibodies.[36–42] In addition to directly computing binding affinities, some of these studies proposed the possibility of allosteric communication between the RBD and the receptor or the antibody,[37,39,42] and showed that dynamical perturbations within the hACE2 receptor can arise due to its binding to the RBD.[43] Such allosteric effects

are key to determining the relative stability of an antigen-antibody complex and can often determine the efficacy of monoclonal antibody based therapeutics. To understand these allosteric communication mechanisms in greater detail, we performed extensive all-atom molecular dynamics (MD) simulations to understand the effect of RBD mutations on the stability, dynamics and the unbinding process of monoclonal antibodies targeted to the SARS-CoV-2 spike protein. Apart from the wild type RBD, we studied three mutant strains with the following mutations: B.1.1.7 (*alpha*) (N501Y), B.1.351 (*beta*) (K417N,E484K,N501Y), and B.1.617 (*kappa*) (L452R,E484Q) . The two antibodies, B38[27] and BD23,[28] were chosen for the current study, because their epitopes contain at least two of the four residues involved in the mutations in the studied variants and also because the new mutations in the *beta* variant have been shown to increase the binding affinity for B38 but decrease it for B23.[36] This contrasting property makes it particularly interesting to understand how the molecular interaction, and the allosteric cross-talk with the RBD, differ between these two mAbs.

Both of these antibodies were first extracted from the plasma of convalescent patients of COVID-19.[27,28] Each is a dimeric protein comprising a heavy and a light chain (labeled as Chain A and B, respectively, in this manuscript) with clearly distinguishable antigen binding domains (Figure 1). The BD23-Fab is smaller in size (126 and 107 residues in the heavy and light chain respectively) compared to the B38-Fab (222 and 218 residues in the heavy and light chain respectively). The epitope of the B38 contains the RBD residues 417 and 501 while the residues 452, 484 and 501 are included in the epitope of BD23. The structures of the RBD-antibody complexes as well as the location of the mutations are depicted in Figure 1.

We studied the effect of RBD mutations on the dynamics of the antigen-antibody complex from three different aspects. First, we demonstrated the relative flexibility of the residues and identified the structural changes taking place in the complex if the RBD of the WT coronavirus is replaced with each of the mutants. Next, we quantified the change in the mutual information based cross-correlation between all pairs of residues and constructed a protein

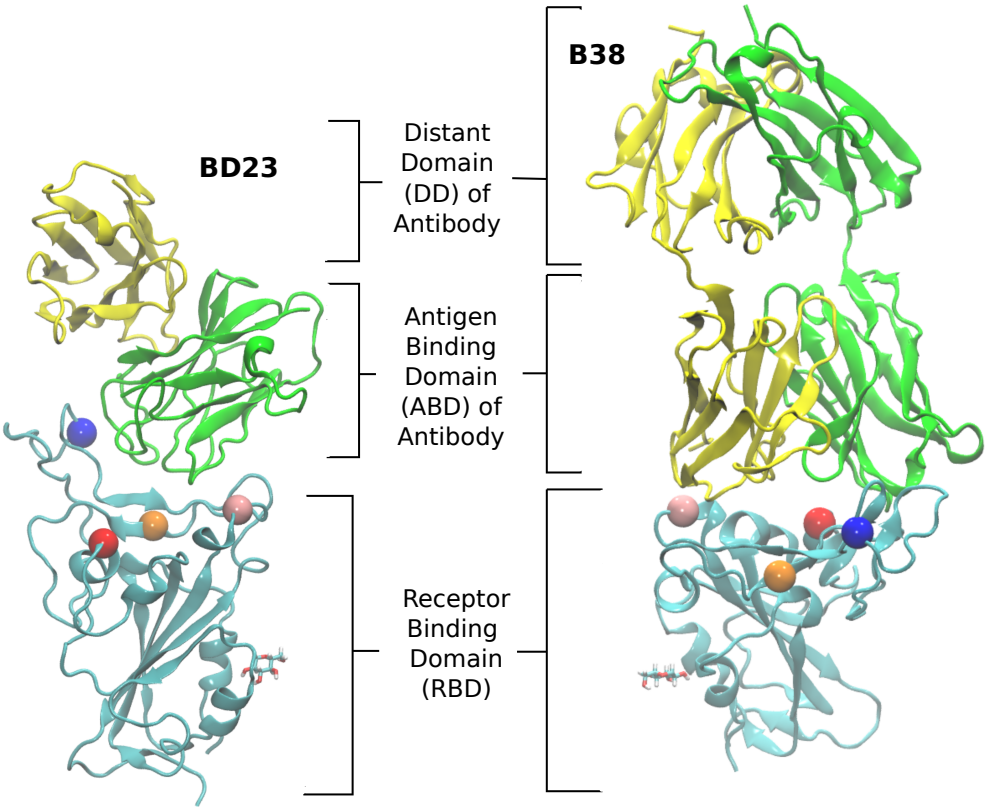

Figure 1: The structure of the RBD-antibody complexes for the two neutralizing antibodies, BD23 and B38-Fab, studied in this work. Each antibody has two chains: the heavy and the light chain. We refer to the heavy chain as chain A and the light chain as chain B. The chain A is colored green and the chain B is colored yellow. The RBD is colored cyan. We define the antigen binding domain (ABD) of the Ab as the domain of the antibody which comes in contact with the RBD. The rest of the antibody is referred to as the distant domain (DD). The Glycan moiety on Asn343 is shown in licorice. The residues which are mutated in the studied variants are represented as colored spheres with the following color scheme: K417 (red), L452 (orange), E484 (blue) and N501 (pink).

graph connectivity network to decipher the modulation of the allosteric information pathways due to mutations in RBD. Finally, we studied the change in the dissociation mechanism of the antigen-antibody complex for all combinations of the mentioned mutant RBDs and the antibodies using non-equilibrium pulling simulations, and rationalized our finding based on the arguments of enthalpy and hydrogen bonding. From the diverse dynamical perturbations observed in these systems, we delineated a few common themes in how the mutations in the SARS-CoV-2 antigen can impart local and global effect through the antibody structure and potentially impair the neutralizing efficacy of monoclonal antibodies.

Computational Methods

System Preparation

The coordinates of the antibodies bound to the receptor binding domain (RBD) of the spike protein in wild type SARS-CoV-2, were obtained from the Protein Data Bank (PDB) with the following accession IDs: 7BZ5 (B38)[27] and 7BYR (BD23).[28] Apart from the B38 antibody, the 7BZ5 PDB file contains the RBD domain (only residues 334-526) including one N-acetyl-β-D-glucosamine (NAG) moiety attached to Asn343. This glycan moiety was preserved in our calculation. The 7BYR PDB file includes the entire spike trimer along with the antibody, so we removed all spike residues except for 334-526 of the RDB bound to the antibody. The bare RBD systems were constructed from the 7BZ5 system by deleting the antibody. The mutations in the RBD were added using CHARMM-GUI input generator.[44] Each system was solvated in a cuboidal water box with 12 Å of padding in each direction, and Na^+ and Cl^- ions were added to neutralize the total charge and maintain an ionic strength of 150 mM. The hydrogen mass repartitioning (HMR) technique[45] was used to allow for 4 fs time-steps facilitating longer simulation runs. The topology files for HMR were prepared using the VMD 1.9.4 alpha 51 software.[46] All systems were modeled using CHARMM36 force field[47] (with CMAP correction for proteins) and TIP3P parameters[48] were used for the

water and the ions.

Equilibration and Unbiased Simulation

Each system was minimized using a conjugate gradient algorithm for 10000 steps followed by an equilibration in NPT ensemble for 250 ps (with 2 fs time step) with harmonic restraint on the alpha carbons of all the protein residues. A 10 ns NPT equilibration was performed (with 4 fs time-step) afterwards for every system with no restraint applied on any atom. The temperature was controlled at 303.15 K using a langevin thermostat with damping constant 1 ps^{-1}, and a Langevin piston was used to control the pressure at 1 atm.

Production runs were performed for each RBD-antibody complex for 0.5 μs and for each bare RBD system for 0.3 μs. For all systems, (WT and three variants), the cumulative unbiased simulation time was 5.2 μs. Only the last 0.4 μs of each antibody bound system and 0.25 μs of each bare RBD system were used for further analysis. All simulations were performed using NAMD 2.14 simulation package.[49] The trajectories were saved at an interval of 100 ps.

The root mean squared deviation (RMSD) and the residue-wise root mean squared fluctuations (RMSF) were computed using the `gmx rms` and `gmx rmsf` tools, respectively, in GROMACS 2018.1 software.[50] RMSD for all systems were computed with respect to the first frame of the long production run. Trajectories were aligned only with respect to the RBD α-carbons using VMD.[46] RMSD was computed for the RBD, antibody, the antigen binding domain (ABD) of the antibody and the whole system. The antigen binding domain is defined as the one of the two monomers of the BD23 protein which interacts with the RBD and the portions of the two monomers directly interacting with RBD (residue 1-108) for the B38 antibody (Fig. 1). For computing RMSF, the last 400 ns of each trajectory is split into 4 segments of 100 ns each. Residue wise RMSF was computed for each segment and the mean and standard deviations are reported. The RMSF ratio is then computed for each mutant strains as the ratio of RMSF for each residue and that of the corresponding residue

in the WT. Principal component analysis was performed using the PyEMMA 2 package.[51] The non-bonding interaction energy (including the electrostatic energy and van-der Waals energy) between the antibody and the mutated residues of the RBD for different variants were calculated using the NAMD Energy module[52] of VMD.[46] Hydrogen bonds between the RBD and antibodies were also analyzed using VMD.

Mutual Information Based cross-correlation and Protein Graph Connectivity Network

Linear mutual information (LMI) based cross-correlation matrices were computed for all residue pairs in each system. The theoretical details can be found in Ref 53–55. Although the LMI based cross-correlation is primarily used to quantify the allosteric effect of a small molecule ligand on the receptor protein,[56,57] it can also be used to decipher the allosteric regulation within a protein or protein complex.[58]

The linear mutual information (LMI) metric (I_{ij}) is calculated as

$$I_{ij} = H_i + H_j - H_{ij} \tag{1}$$

where H is a Shannon type entropy function:

$$\begin{aligned} H_i &= -\int p(\mathbf{x}_i) \ln p(\mathbf{x}_i) d\mathbf{x}_i \\ H_{ij} &= -\int\int p(\mathbf{x}_i, \mathbf{x}_j) \ln p(\mathbf{x}_i, \mathbf{x}_j) d\mathbf{x}_i d\mathbf{x}_j \end{aligned} \tag{2}$$

$\mathbf{x}_i, \mathbf{x}_j$ are the vectors containing the Cartesian coordinates of the C_α atoms, $p(\mathbf{x}_i)$ and $p(\mathbf{x}_j)$ are their marginal distributions and $p(\mathbf{x}_i, \mathbf{x}_j)$ is the their joint distribution.[55,57] A Pearson like correlation coefficient C_{ij} is defined from I_{ij} in the following manner:

$$C_{ij} = (1 - e^{-(2/d)I_{ij}})^{-1/2} \tag{3}$$

where d is the dimensionality of the space. Unlike the conventional correlation coefficient, C_{ij} defined by Eq. 3 can only take values between zero and one.

The residue-wise cross-correlation matrices were averaged over the four 100 ns segments prepared from the last 400 ns of each unbiased production run. The changes of the cross-correlation across the mutants were used to decipher the role of the mutations in the large scale dynamics. We also constructed a protein graph connectivity network model based on the cross-correlation matrices. The α-carbon of each residue is considered as the nodes of the graph and the cross-correlation between residues as the weight of the edges. Two residues were considered connected only if the heavy atoms of those residues were within 5 Å of each other during at least 75 % of the entire production run. The betweenness centrality (BC) of each residue in the network was computed and compared between various mutant strains. The BC quantifies the information flow between nodes or edges of a network. As the α-carbon of each residue is a node in the protein-graph-connectivity network, the value of the BC denotes the functional relevance of each residue in the dynamics of allosteric information flow through the protein chains. If a node, i, functions as a bridge between two other nodes along the shortest path joining those two, the BC of the node i is

$$BC(i) = \sum_{st} \frac{n^i_{st}}{g_{st}}, \tag{4}$$

where g_{st} is the total number of geodesics a.k.a. the shortest paths joining nodes s and t, out of which n^i_{st} paths include the node i.[56–58] The change in BC, due to RBD mutations, is used to quantify the dynamical role of mutations in modifying the information flow pathway in the RBD-spike complex. The LMI based cross-correlations were calculated and the protein graph connectivity networks were constructed using the bio3D package.[59]

Steered Molecular Dynamics Simulation

To study the unbinding of the antibodies from the spike RBD, steered molecular dynamics (SMD) simulations[60] were performed. A fictitious particle was attached to the pulling coordinate (center of mass distance between RBD and antibody) with a harmonic spring (1 kcal/mol/Å) to allow for sufficient fluctuations. For SMD simulation, all systems were modeled with the Generalized Born (GB) implicit solvent model[61] with solvent accessible surface area (SASA) correction (GBSA). The ion concentration was set at 0.15 M. The pulling was performed at a constant speed of 4 Å/ns. Five SMD trajectories of 10 ns length were generated for each system. Each trajectory was saved at an interval of 10 ps, and the pulling force and the accumulated work were recorded every 0.1 ps. The starting structures for the SMD trajectories were sampled from the unbiased production runs at the following points: 300 ns, 350 ns, 400 ns, 450 ns and 500 ns. All SMD simulations were started without further equilibration. The colvars[62] module in conjunction with NAMD 2.14[49] was used for SMD simulations.

Results

Modulation of conformational flexibility

The RBD, with or without the antibody, is a relatively rigid system (RMSD $\sim$ 2-3 Å) with less conformational variability, likely due to the abundance of beta-sheets in the structure. The antibodies on the other hand are highly flexible and often show large conformational fluctuations, as indicated by their high root mean squared deviation (RMSD) (see supporting information) values throughout the production runs. Unlike the BD23 system where the entire antibody is highly flexible, in the case of B38, the fluctuations are significantly larger in the distant domain (DD), compared to the antigen binding domains for both chains. The RBD-Ab complexes of both the WT and mutants, are also capable of exploring multiple free

energy minima during the rather short 0.4 μs period as demonstrated by the projection of their dynamics on the first two principal components. But any discernible difference between the dynamics of the WT and mutant complexes is not apparent from the RMSD and PCA analysis. However, the RMSF of certain residues of both the RBD and Ab show significant change going from WT to the mutants. To demonstrate this effect, we computed the ratio of RMSF of each residue for every mutant with that of the WT system. Even in the case of the bare RBD system, the region comprising residues 460-510 shows increased flexibility in the L452R-E484Q variant and decreased flexibility in the N501Y mutant. Interestingly, two of the concerned mutations, E484Q and N501Y, are present within this region, which also interacts directly with both the B38 and BD23 antibodies. The change in flexibility, upon mutation, is the highest in the loop formed by residues 470-490, going up or down by a factor of 2-3 in the B.1.617 or the B.1.1.7 variants respectively. The individual mutated residues show a sharp change in RMSF values, particularly in the residue 452, 484 and 501 in the respective variants. This effect is also visible in the antibody bound systems, where the mutated residues show sharp peaks in the RMSF ratio plot (Fig. 2d and j). The residue 484 shows a contrasting behavior in the presence of B38 and BD23 antibody. When in complex with B38-Fab, K/Q484 and adjacent residues show a large increase in flexibility ($\sim$2 times that of E484 in WT) but they become almost twice more rigid when bound to BD23. On average, the RBD, with the L452R-E484Q mutations, in comparison to the WT, becomes the most structurally rigid when bound to either antibody but the most flexible when unbound. The N501Y mutant and the K417N-E484K-N501Y mutant show the largest increase in overall flexibility in the presence of BD23 and B38-Fab respectively, but their RMSF remain virtually unchanged with respect to the WT RBD in the absence of any antibody.

More interesting is the change in RMSF in the antibody, as it serves as a direct proof that secondary perturbations arising from mutations in the antigenic epitope can influence the microscopic dynamics of the antibody. The change in the residue wise RMSF of both the

antibodies are, as expected, less dramatic, compared to that in the RBD, as these changes come due to a secondary perturbation caused by mutations outside the protein domain via non-covalent interactions (Fig. 2e and i).

In Fig. 2 we depict the ratio of the RMSF of the antibodies in complex with the mutant RBDs with respect to their wild type counterparts. For B38-Fab, the deviation is small (RMSF ratio within 0.5-1.5), except for specific residues in the distant domain, when bound to the L452R-E484Q mutant. But the changes in flexibility are much more prominent for the BD23 antibody, for which, RMSF increases on average, in response to a N501Y mutation in the *alpha* variant, but the effect is largely compensated by the K417N and E484K mutations in the *beta* variant, bringing the RMSF down to a level comparable to a WT complex. The L452R and E484Q mutation in the B.1.617 strain causes an increase in overall rigidity of the antibody structure, particularly in the distant domain.

Change in correlated motion and allosteric information flow

Significant changes in the residue wise LMI based cross-correlation can be observed throughout the complex (both RBD and antibody) in presence of the RBD mutations (see Supporting information). We particularly focus here on the cross-correlation coefficient between the RBD and the antibody residues, as this can provide a direct quantitative idea about how their motions are coupled or decoupled. In Fig. 3 we depict the relative RDB-antibody cross-correlation for each mutant system, with respect to the WT complex. One of the key features of the B38-Fab is that Ab residues show significantly large change in correlation with the mutated RBD residues and the residues adjacent to the mutation. For example, in the N501Y variant, many residues of B38 Ab show a decrease in correlation, by 0.1-0.2, with the residue 501 and its nearby RBD residues. More interestingly, this effect is propagated over a long distance, even to the distant domains of the antibody, indicating that single point mutations in RBD can have a strong long range perturbative effect on the dynamics of the antibody bound to the RBD. A similar phenomenon is observed for N417 and its neighboring

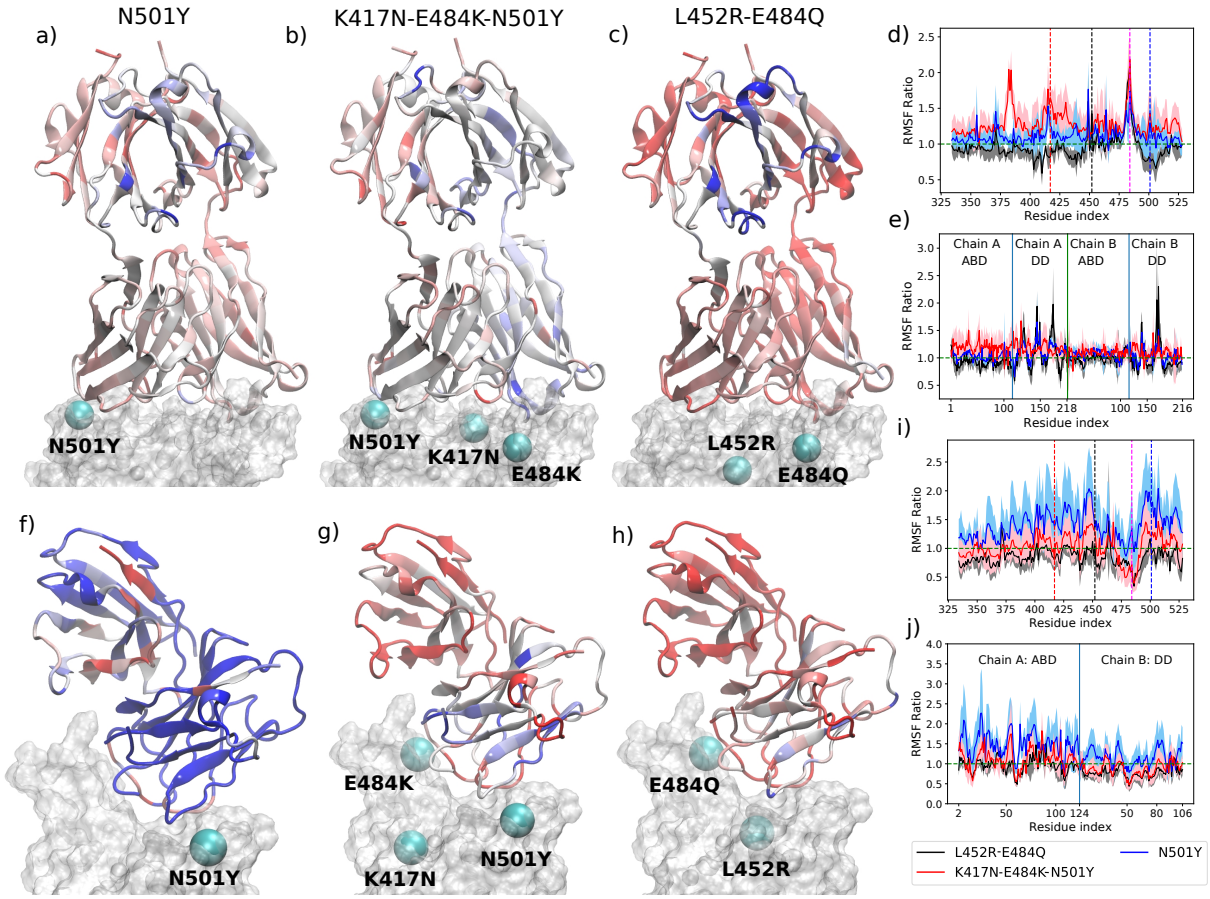

Figure 2: Change of root mean squared fluctuation (RMSF) of the RBD-Ab complex due to the mutations in the variants. The RBD is represented by a transparent surface. The mutated residues are shown as cyan spheres. The antibody residues are colored according to the ratio of their RMSF when bound to a mutant RBD with that of the WT case. Blue color indicates increase in RMSF and red color indicates decrease in RMSF. The residue RMSF ratio is projected on the structure of the B38-Ab complex for (a) N501Y, (b) K417N-E484K-N501Y, and (c) L452R-E484Q variants. The RMSF ratio for just the RBD is shown in (d) and for the B38 antibody in (e). The figures (f-j) are identical to (a-b) but are for the BD23-Fab. In figure (d) and (i), the location of the mutations are shown as vertical dashed lines.

residues (410-420) in the K417N-E484K-N501Y mutant, the R452 and its nearby residues (440-455), and for the Q484 residue in case of the L452R-E484Q mutant. Although this effect is much less pronounced in the BD23-Fab, the change in cross-correlation coefficient with the mutated RBD residues is indeed observed when, for example, in complex with the K417N-E484K-N501Y mutant. Unlike B38, this effect is much less uniform within the antibody, where certain groups of residues (e.g. near residue 50, 70 and 100 in the ABD), show large change of correlation with the mutated residues as well as for the whole RBD.

Moreover, there is, on average, an increase in the cross-correlation between the RBD and the B38 antibody, going from the *alpha* variant to the *beta* variant while the trend is reversed for BD23. Previous computational studies have established that B38 binds more weakly with the spike of the *alpha* variant compared to the *beta* variant, but BD23 binds at least twice as strongly to *alpha* variant than to the *beta* variant.[36,38] This observation indicates the mutual information based cross-correlation and the binding affinity between the monoclonal antibodies and the spike epitopes follow a similar trend.

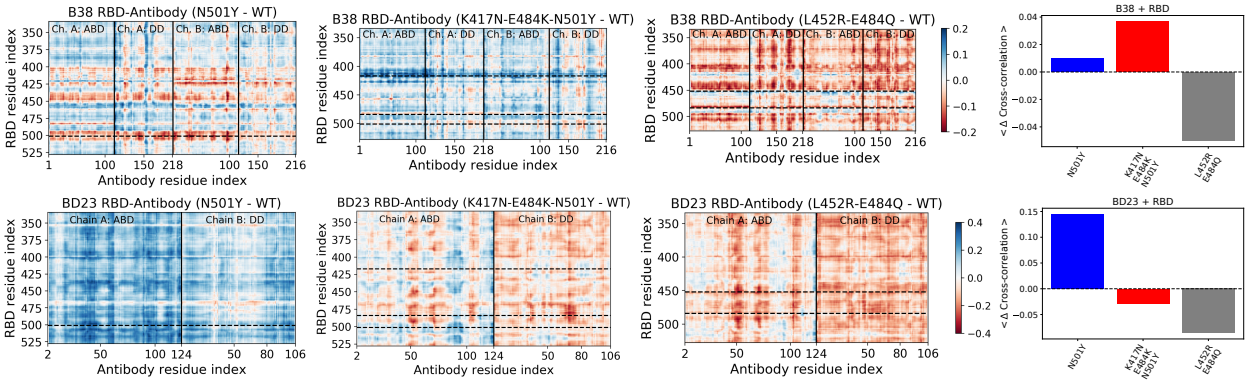

Figure 3: Change in the mutual information based cross-correlation between the antibody and the RBD residues, due to the mutations in the variants. The differences are reported as the cross-correlations of the WT species subtracted from that of the mutant species. The locations of specific mutations are labelled as dashed horizontal lines. The continuous vertical lines separate different domains and chains of the protein (for details see figure 1). The residue-wise average change in cross-correlation values for each system is depicted in the rightmost column

This contrasting effect in the correlated motion and the binding affinity indicate that the flow of dynamical information between residues, takes very different pathways in the

two antibodies. To probe these pathways, we built a protein graph-connectivity network model, treating each residue as the node and the cross-correlation between the residues as the weights of the edges of the graph. We computed the betweenness centrality (BC) measure, a metric which computes the relative importance of each node in the information flow pathway. We then computed the residue wise difference of BC in each mutant relative to the WT system. Changes in BC point us to the residues which either gain or lose importance in the allosteric information flow pathway in the protein. In B38-Fab, significant changes in the BC metric is primarily limited to the residues of the antigen binding domain, showcasing a situation where local correlation propagates through the amino acid sequences, leading to long range dynamical changes. Particularly, we see a large increase in the BC value for a few consecutive residues in the region of residues 92-98 in the chain A, and a large decrease in the BC for residues 23-30 in chain B, for all the mutant species. This imbalance is primarily caused by the differential interaction of the 501 residue in its WT (N501) compared to its mutated form (Y501). The change in BC in chain B is reduced by a significant amount when the N501Y mutation is removed, as in the L452R-E484Q variant. This effect can be a result of the reduced interaction energy of Y501 with the B38 mAb as well as the loss of the hydrogen bond between the RDB N501 residue and the S30 residue of chain B of B38, although, there is an overall increase in the hydrogen bond occupancy for Y501 as the lost bond is replaced by a hydrogen bond with S67. In essence, the allosteric information flow through the B38 antibody follows a re-wiring mechanism. The mutations switch off the information flow pathway along the residues 23-30 in chain B and increases the information traffic along residues 92-98 in chain A. This effect is highly asymmetric, leading to a drop or rise of the cross-correlation of all antibody residues with particular mutated residues in RBD.

Unlike the B38, in BD23-Fab, a large fraction of the RBD-mAb interface, specifically the residues 97-107 of the ABD, loses centrality along with some isolated distant domain residues, which is a common theme across all mutants. Reduction of BC is also observed

for residues 40-50 in the ABD and residues 80-90 in the DD, indicating the possibility of long distance propagation of allosteric signal. But the dynamical effect is different from that in the B38, as the perturbation is not localized in the vicinity of any specific mutation. The same set of residues experiences a decrease in centrality measure, irrespective of the specific location and the nature of the mutation (except for the N501Y variant, where some residues show a gain in BC, particularly the ABD 45-50 and DD 85-90). This qualitatively explains why we observe mutation-specific long distance correlation changes in the case of B38 (horizontal correlation changes in Fig. 3), whereas in BD23, certain residues lose or gain correlation with almost all residues of the RBD and not particularly the mutated ones (vertical correlation changes in Fig. 3).

Dissociation dynamics and interactions at the RBD-Antibody interface

From multiple steered molecular dynamics simulations (SMD), we elucidated the unbinding mechanism of the monoclonal antibodies from the spike RBD. For detailed inspection, we picked the pathway that corresponds to the lowest amount of non-equilibrium work for each RBD variant and mAb combination, as it would contribute the most to the real unbinding process. For all variants and both the antibodies, the loop consisting of residues 470-490 is found to play an important role in the unbinding process. It is the last point of contact between the RBD and the antibody in the lowest work dissociation pathway for every system, and it functions like an anchor to adhere to the antibody before a complete detachment occurs. Unsurprisingly, one of the key mutating residue (E484) is situated in this region of the RBD, and, when not mutated, it is often the last RBD residue that forms a hydrogen bond with the dissociating antibody. But in the K417N-E484K-N501Y and L452R-E484Q variants, this residue is mutated and no longer forms the "last" hydrogen bond to anchor the departing antibody. Instead, other residues from the same loop, primarily S477, which has a hydroxyl side-chain, performs the role. We also observed A475 to form the "last" hydrogen

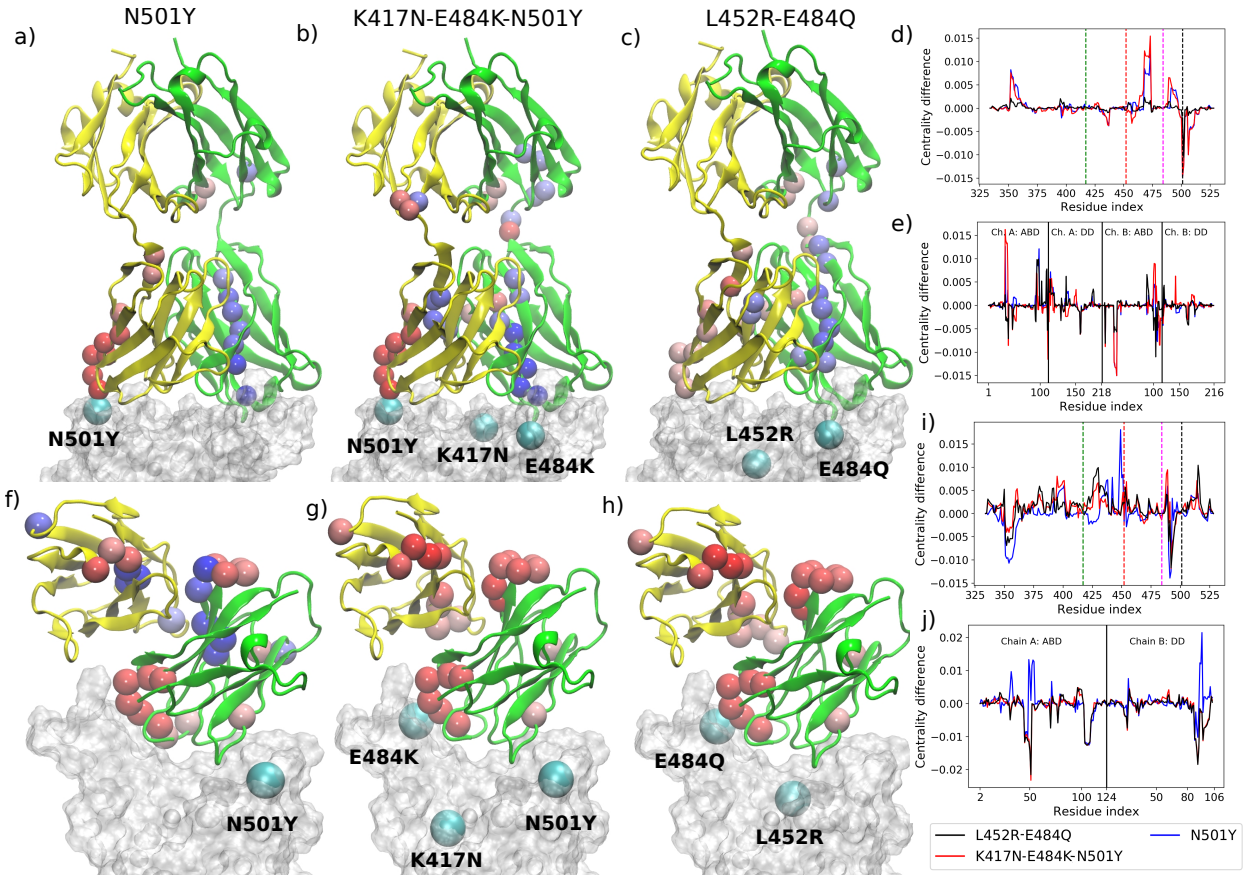

Figure 4: Change of betweenness centrality (BC) of each residue of the RBD-Ab complex due to the mutations in the variants. The RBD is represented by a transparent surface. The mutated residues are shown as cyan spheres. Only residues with a change in BC of greater than 0.005 is shown in colored sphere. Blue color indicates increase in BC and red color indicates decrease in BC. The residue wise BC change is projected on the structure of the B38-Ab complex for (a) N501Y, (b) K417N-E484K-N501Y, and (c) L452R-E484Q variants. The BC change for just the RBD is shown in (d) and for the B38 antibody in (e). The figures (f-j) are identical to (a-b) but are for the BD23-Fab. In figure (d) and (i), the location of the mutations are shown in vertical dashed lines.

bond for the L452R-E484Q RBD with B38 antibody, with its main chain hydrogen bond donor group (See supporting information).

We computed the average non-equilibrium work required to detach the antibody for all systems, as $-\ln\langle\exp(-W_i)\rangle$, where W_i denotes the accumulated work in the ith SMD run, and $\langle\rangle$ indicates arithmetic mean. The average work is heavily dominated by the dissociation path that requires the lowest amount of work. In the limit of infinite number of pulling trajectories or in the limit of infinitely slow pulling, the average non-equilibrium work will become equal to the unbinding free energy. Provided E484 is the key anchoring residue, we expect the non-equilibrium work will depend on how strongly this particular residue or its mutants interact with the antibody. From the non-bonded energy calculation on the equilibrium trajectory it is apparent that the three mutated residues: E484, K484 and Q484, have little difference in their interaction energy with the B38-Fab antibody, primarily because this residue is not in direct contact with the antibody interface (Fig. 5b). Consequently, the three mutants do not show any discernible difference in the work required for the dissociation of the RBD-mAb complex (Fig. 5c). But all the mutants require less work for antibody detachment in comparison to the WT, an effect that can partially be attributed to the N501Y mutation. From non-bonded energy calculation we see that the N501Y mutation destabilizes the interaction between RBD and B38 by lowering (less negative) the interaction energy (see Supporting information).

For the BD23-Fab, an almost opposite effect is observed. The residue E484, being situated in the RBD-mAb interface, plays a key stabilizing role for the complex via hydrogen bond to the S103 and S104 residues of the Ab. Once mutated, the hydrogen bond propensity of residue 484 diminishes, leading to almost 80 kcal/mol decrease (less negative) in the non-bonded interaction energy with the mAb, in agreement with a recent computational study.[38] The E484 forms hydrogen bonds with the S104 (26.37% with backbone and 54.19% with side-chain) and S103 (3.85% with backbone and 8.62% with side-chain) residues of BD23 with high occupancy in the WT and with G102 (31.9%), S103 (4.15%), Y32(10.7%), Y110 (3.95%)

and Y111 (2.73%) residues of the antibody in the N501Y mutant. In the K417N-E484K-N501Y variant, K484 forms hydrogen bonds only with N92 (6.86%) and Y110 (1.18%) with relatively low occupancy. This effect is clearly reflected in the non-equilibrium work profile, where, going from N501Y mutant to K417N-E484K-N501Y and L452R-E484Q variants, we see a significant drop in the work required for the detachment of the antibody. But the N501Y mutant binds more strongly with the BD23-Fab (Figure 5f) compared to the WT, because the non-bonding interaction energy of Y501 is higher (more negative) than that of the N501 residue (Supporting info). This effect can be attributed to the increased probability of hydrogen bonding between the RBD and the antibody by the Y501 residue compared to the N501. In the WT system, N501 participates in one hydrogen bond with the D73 residue of the BD23-Fab with negligible occupancy (0.62%). But in the N501Y mutant, the Y501 participates in two hydrogen bonds with the L72 and the Y80 residues of the antibody with significantly higher occupancy (5.77% and 6.27% respectively). The rupture forces of the spike antibody complexes follow a similar trend as the average non-equilibrium work for the WT and the mutants (see Supporting Information).

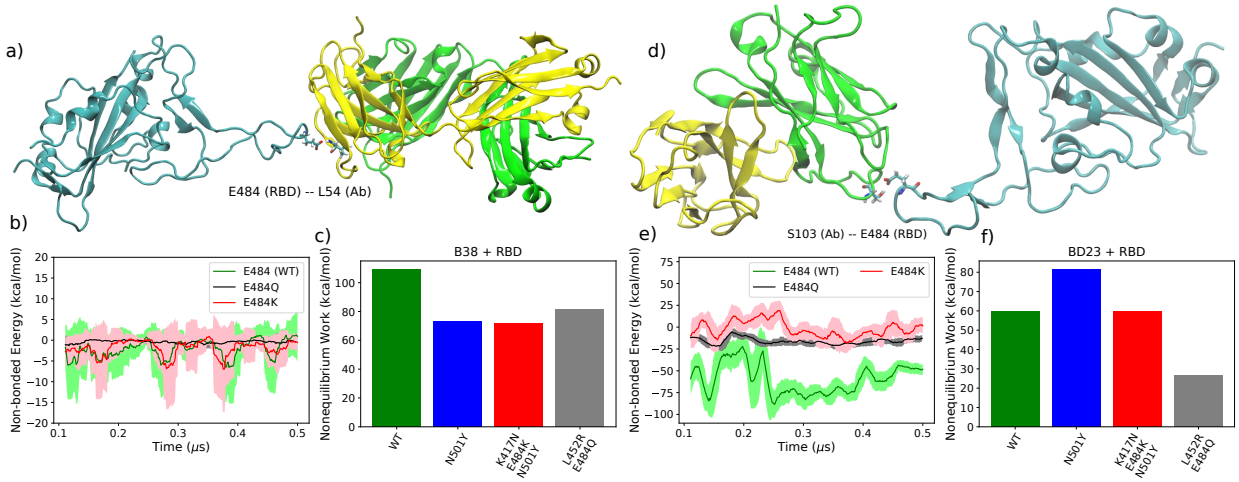

Figure 5: (a) A representative intermediate structure for the B38 antibody unbinding from the RBD from the SMD simulation. Intermediates for all variants are shown in supporting information. (b) The non-bonded interaction energy between the RBD residue 484 and the B38 antibody from the unbiased simulation. (c) The average non-equilibrium work performed to dissociate the B38 antibody from all variants of the RBD using SMD simulation. Figure (d-f) are identical as (a-c) but for BD23 antibody.

Discussions and Conclusions

We performed atomistic molecular dynamics simulations of the receptor binding domain of the SARS-CoV-2 spike protein in complex with neutralizing antibodies to understand the role of spike RBD mutations in immune evasion, via perturbing the microscopic dynamics of the antibodies. We specifically focused on three mutant strains with the following mutations in the RBD: *alpha* variant or B.1.1.7 strain (N501Y), *beta* variant or B.1.351 strain (K417N-E484K-N501Y), and the *kappa* variant or B.1.617 strain (L452R-E484Q), a precursor to the highly infectious B.1.617.2 strain or the *delta* variant. We studied the conformational dynamics of each of these mutant RBD domains bound to two monoclonal antibodies: the B38-Fab and the BD23-Fab. Comparing the results with identical simulations of the WT RBD, we uncovered some distinctive features.

First, the structures of the antibodies are largely flexible and can undergo significant conformational transitions within a few hundred ns timescale. But the flexibility of certain residues in the antigen-antibody complex are modified disproportionately when the WT RBD is replaced with one from the mutant strains. Inside the RBD, the residues which are mutated and the ones proximal to the mutation show the largest change in flexibility, measured as the root mean squared fluctuation (RMSF). Particularly, in the bare RBD, the loop involving residues 470-490 becomes flexible when residue 484 becomes incapable of forming a stabilizing hydrogen bond upon mutating from Glu to Lys or Gln. There are striking long distance effects of the reduction or increase in flexibility, propagating deep into the antibody structure. Apart from the antigen binding domain (ABD), we observe noticeable changes in rigidity of the distant domains of both antibodies. This effect is more prominent for the smaller sized BD23 antibody, where the N501Y mutation dramatically increases the dynamic motion throughout the antibody structure. The K417N and E484K mutations reverse this effect to a large extent, and in the B.1.617 variant, both the antibodies become structurally more rigid as compared to the WT complex. This result is particularly important because, despite the absence of any mutation in the antibody itself, single point

mutations in the antigen epitope are observed to significantly perturb the dynamics of the antibody and potentially impact the stability of the antigen-antibody complex. It is an indication that there exists an allosteric communication between the RBD and the antibody.

One of the best ways to quantify allosteric effects in a protein is via cross-correlation between residues. We computed the linear mutual information based cross-correlation between every pair of residues for all RBD-antibody combinations, explored in this work. Cross-correlation values, for both the RBD and the antibody, can change significantly if the WT RBD is replaced with a mutant one. But there are contrasting features in how this change takes place in the two antibodies. In B38-Fab, almost all residues either gain or lose correlation with the mutated residues in the RBD. In the RBD antibody cross-correlation difference plots, this effect is pronounced as horizontal lines. It often spans across the entire antibody, even reaching up to the distant domains, reflecting the appearance of long distance propagation of allosteric signal. We previously observed such an effect within the spike protein,[58] but now we see that the allosteric effect can be propagated into the antibodies that interact with the spike only via non-covalent interactions.

For BD23, the coupling between the RBD and the antibody follows a different pattern than that in B38. Certain groups of residues in the BD23-Fab, gain or lose correlation with the entire RBD and not just with the mutated residues. The antibody residues impacted by the mutation are conserved for all mutants, but whether they show a positive or negative change in cross-correlation can depend on the nature of the mutation. For example, the correlation increases in the presence of the single N501Y mutations, but in the other two variants with multiple other mutations, the RBD and antibody dynamics become more decorrelated. In this connection, one key observation is that the gain or loss in cross-correlation seems to follow the trend of binding affinity. This phenomenon demands a thorough future investigation of the relationship between the binding free energy and the inter-residue cross-correlations for a wide range of protein-protein complexes.

To get a deeper understanding of the information flow pathway inside the antibody, we

constructed a protein graph connectivity network for each system and computed the betweenness centrality (BC) of each residue to understand its role in the allosteric information propagation. We specifically looked at the change in the BC value for the antibody residues when mutations are introduced into the antigen (spike RBD). We observed that in the case of the B38 antibody, a set of amino acids in the light chain, proximal to RBD residue 501, is experiencing a loss in centrality while the centrality is increased in virtually the opposite end of the antibody i.e. in the part of heavy chain near RBD interface. This effect is reduced when the N501 remains unmutated as in the case of the L452R-E484Q variant. So, the net result of the mutations is some kind of re-wiring mechanism, as the traffic of allosteric information flow is reduced in the amino acids near the N501Y mutation and increased near the K417N and E484K/Q mutations. This effect is strongly dependent on the location of the mutated residue in the RBD. It can explain the observation of long distance perturbation of the cross-correlation between mutated RBD residues and the B38 antibody. For the BD23-Fab, the effect is very different. Antibody residues near the binding interface experience a reduced centrality, irrespective of the specific location of the mutations. Some residues in the distant domain also show a change in BC value and, similar to the interface residues, they do not depend on the specific location of the mutations in RBD. This explains why we see specific residues in the BD23-Fab, gain or lose correlation with the entire RBD. These contrasting features show that there can be inherent differences in the microscopic dynamics of the antibody, depending on the nature of mutations in the antigen and on the nature of the antibody. This can have repercussions beyond the specific SARS-CoV-2 spike antigen and to the fundamental process of antigen-antibody recognition in general.

Another process, of significant interest, is the unbinding mechanism of the antibodies from the spike proteins of different variants; it can provide us a molecular level knowledge of how the antibody binding might be impaired by the variants and is of paramount importance in reaching population-scale herd immunity via vaccination. The RBD loop, consisting of residues 470-490, functions like an anchor and is always the last region to interact with

the antibody in the lowest energy dissociation pathways, irrespective of the variant or the antibody. The mutation that arises in this region is the E484K or the E484Q, both of which reduces the anchoring capability with the BD23 antibody by the loss of key hydrogen binding interactions. So, the N501Y, K417N-E484K-N501Y, and L452R-E484Q mutants show a decreasing trend in the non-equilibrium work required to dissociate the BD23 antibody, (the difference between the last two variants can be attributed to the reduced stabilization via non-bonded interaction between R452 and the antibody). B38, in contrast, does not interact with residues 484 or 452 in the bound state, and mutations in those residues have little impact on the interaction energy of B38 with the spike protein. So, the N501Y, K417N-E484K-N501Y, and L452R-E484Q mutants require virtually identical amount of work for the unbinding of the B38 antibody. But the mutants have lower "binding strength" than the WT because of the loss of stabilizing hydrogen bonds as a result of the N501Y mutation. Interestingly, the newly emerging highly contagious *delta* variant or B.1.617.2 strain (L452R-T478K) and the *delta plus* variant (K417N-L452R-T478K) also gained a different mutation in this important loop region (RBD residues 470-490) that is vital in preventing the dissociation of the antibody.

In summary, we quantified how the microscopic dynamics of the antigen-antibody complex is perturbed by to mutations in the antigen and the nature of the antibody, with a particular focus on the SARS-CoV-2 spike protein, to address the challenge from the recent pandemic. Although there is significant diversity in the dynamical perturbations observed in the molecular level, there are some common fundamental themes: modulation of inter-residue correlations, allosteric information propagation, and destabilization of non-bonded interactions. The results of this study can guide us to explain the binding propensity and the overall stability of the antigen-antibody complexes in general and the immune response against the coronavirus in particular. Future studies in this direction can lead to a deeper understanding of the immune evasion mechanism of mutating viruses and can help in designing adaptive therapeutic strategies against new viral strains by immunization through

monoclonal antibodies and vaccination.

Acknowledgement

The authors thank Ly Le, Trevor Gokey, Sharon Stone, and Moises Romero for their suggestions and feedback on the manuscript. This work was supported partially by the National Science Foundation (NSF) via grant MCB 2028443. The authors thank the Triton Shared Computing Cluster (TSCC) in San Diego Supercomputer Center (SDSC), and UC Irvine High Performance Computing (HPC) facility for providing the computational resources. The authors declare no competing financial interest.

Data Availability Statement

All the trajectory data and the analysis scripts will be made available via Zenodo and GitHub respectively.

Supporting Information Available

Table S1: List of each simulation performed in this study

Figure S1-S20: Additional figures.

References

(1) Zhou, P. et al. A pneumonia outbreak associated with a new coronavirus of probable bat origin. *Nature 2020 579:7798* **2020**, *579*, 270–273.

(2) COVID Live Update: 192,878,212 Cases and 4,143,593 Deaths from the Coronavirus - Worldometer. `https://www.worldometers.info/coronavirus/#countries`.

(3) Hsieh, C.-L. et al. Structure-based design of prefusion-stabilized SARS-CoV-2 spikes. *Science* **2020**, *369*, 1501–1505.

(4) Andreano, E. et al. SARS-CoV-2 escape in vitro from a highly neutralizing COVID-19 convalescent plasma. *bioRxiv* **2020**, 2020.12.28.424451.

(5) Serapian, S. A.; Marchetti, F.; Triveri, A.; Morra, G.; Meli, M.; Moroni, E.; Sautto, G. A.; Rasola, A.; Colombo, G. The Answer Lies in the Energy: How Simple Atomistic Molecular Dynamics Simulations May Hold the Key to Epitope Prediction on the Fully Glycosylated SARS-CoV-2 Spike Protein. *The Journal of Physical Chemistry Letters* **2020**, *11*, 8084–8093.

(6) Starr, T. N. et al. Antibodies to the SARS-CoV-2 receptor-binding domain that maximize breadth and resistance to viral escape. *bioRxiv* **2021**, 2021.04.06.438709.

(7) Aaron Morris,; William McCorkindale,; Moonshot Consortium, T. C.; Nir Drayman,; D. Chodera, J.; Savaş Tay,; Nir London,; A. Lee, A. Discovery of SARS-CoV-2 main protease inhibitors using a synthesis-directed de novo design model. *Chemical Communications* **2021**, *57*, 5909–5912.

(8) Tai, W.; He, L.; Zhang, X.; Pu, J.; Voronin, D.; Jiang, S.; Zhou, Y.; Du, L. Characterization of the receptor-binding domain (RBD) of 2019 novel coronavirus: implication for development of RBD protein as a viral attachment inhibitor and vaccine. *Cellular & Molecular Immunology 2020 17:6* **2020**, *17*, 613–620.

(9) Ou, X. et al. Characterization of spike glycoprotein of SARS-CoV-2 on virus entry and its immune cross-reactivity with SARS-CoV. *Nature Communications 2020 11:1* **2020**, *11*, 1–12.

(10) Rogers, T. F. et al. Isolation of potent SARS-CoV-2 neutralizing antibodies and protection from disease in a small animal model. *Science* **2020**, *369*, 956–963.

(11) Li, W. et al. Rapid identification of a human antibody with high prophylactic and therapeutic efficacy in three animal models of SARS-CoV-2 infection. *Proceedings of the National Academy of Sciences* **2020**, *117*, 29832–29838.

(12) Zost, S. J. et al. Potently neutralizing and protective human antibodies against SARS-CoV-2. *Nature* **2020**, *584*, 443–449.

(13) Jiang, S.; Zhang, X.; Du, L. Therapeutic antibodies and fusion inhibitors targeting the spike protein of SARS-CoV-2. *https://doi.org/10.1080/14728222.2020.1820482* **2020**,

(14) Chowdhury, R.; Adury, V. S. S.; Vijay, A.; Singh, R. K.; Mukherjee, A. Atomistic De-novo Inhibitor Generation-Guided Drug Repurposing for SARS-CoV-2 Spike Protein with Free-Energy Validation by Well-Tempered Metadynamics. *Chemistry – An Asian Journal* **2021**, *16*, 1634–1642.

(15) Smith, M.; Smith, J. C. Repurposing Therapeutics for COVID-19: Supercomputer-Based Docking to the SARS-CoV-2 Viral Spike Protein and Viral Spike Protein-Human ACE2 Interface. **2020**,

(16) Han, Y.; Král, P. Computational Design of ACE2-Based Peptide Inhibitors of SARS-CoV-2. *ACS Nano* **2020**, *14*, 5143–5147.

(17) Polack, F. P. et al. Safety and Efficacy of the BNT162b2 mRNA Covid-19 Vaccine. *https://doi.org/10.1056/NEJMoa2034577* **2020**, *383*, 2603–2615.

(18) Baden, L. R. et al. Efficacy and Safety of the mRNA-1273 SARS-CoV-2 Vaccine. *https://doi.org/10.1056/NEJMoa2035389* **2020**, *384*, 403–416.

(19) Voysey, M. et al. Safety and efficacy of the ChAdOx1 nCoV-19 vaccine (AZD1222) against SARS-CoV-2: an interim analysis of four randomised controlled trials in Brazil, South Africa, and the UK. *The Lancet* **2021**, *397*, 99–111.

(20) Correia, I. Stability of IgG isotypes in serum. *mAbs* **2010**, *2*, 221–232.

(21) Rabia, L. A.; Desai, A. A.; Jhajj, H. S.; Tessier, P. M. Understanding and overcoming trade-offs between antibody affinity, specificity, stability and solubility. *Biochemical Engineering Journal* **2018**, *137*, 365–374.

(22) Davis, C. W. et al. Longitudinal Analysis of the Human B Cell Response to Ebola Virus Infection. *Cell* **2019**, *177*, 1566–1582.

(23) Taylor, P. C.; Adams, A. C.; Hufford, M. M.; Torre, I. d. l.; Winthrop, K.; Gottlieb, R. L. Neutralizing monoclonal antibodies for treatment of COVID-19. *Nature Reviews Immunology 2021 21:6* **2021**, *21*, 382–393.

(24) Barnes, C. O. et al. Structures of Human Antibodies Bound to SARS-CoV-2 Spike Reveal Common Epitopes and Recurrent Features of Antibodies. *Cell* **2020**, *182*, 828–842.

(25) Liu, L. et al. Potent neutralizing antibodies against multiple epitopes on SARS-CoV-2 spike. *Nature 2020 584:7821* **2020**, *584*, 450–456.

(26) Hansen, J. et al. Studies in humanized mice and convalescent humans yield a SARS-CoV-2 antibody cocktail. *Science* **2020**, *369*, 1010–1014.

(27) Wu, Y. et al. A noncompeting pair of human neutralizing antibodies block COVID-19 virus binding to its receptor ACE2. *Science* **2020**, *368*, 1274–1278.

(28) Cao, Y. et al. Potent Neutralizing Antibodies against SARS-CoV-2 Identified by High-Throughput Single-Cell Sequencing of Convalescent Patients' B Cells. *Cell* **2020**, *182*, 73–84.

(29) Zhou, D. et al. Structural basis for the neutralization of SARS-CoV-2 by an antibody from a convalescent patient. *Nature Structural & Molecular Biology 2020 27:10* **2020**, *27*, 950–958.

(30) Lv, Z. et al. Structural basis for neutralization of SARS-CoV-2 and SARS-CoV by a potent therapeutic antibody. *Science* **2020**, *369*, 1505–1509.

(31) Huo, J. et al. Neutralizing nanobodies bind SARS-CoV-2 spike RBD and block interaction with ACE2. *Nature Structural & Molecular Biology 2020 27:9* **2020**, *27*, 846–854.

(32) Leung, K.; Shum, M. H.; Leung, G. M.; Lam, T. T.; Wu, J. T. Early transmissibility assessment of the N501Y mutant strains of SARS-CoV-2 in the United Kingdom, October to November 2020. *Eurosurveillance* **2021**, *26*, 2002106.

(33) Graham, M. S. et al. Changes in symptomatology, reinfection, and transmissibility associated with the SARS-CoV-2 variant B.1.1.7: an ecological study. *The Lancet Public Health* **2021**, *6*, e335–e345.

(34) Greaney, A. J.; Loes, A. N.; Crawford, K. H.; Starr, T. N.; Malone, K. D.; Chu, H. Y.; Bloom, J. D. Comprehensive mapping of mutations in the SARS-CoV-2 receptor-binding domain that affect recognition by polyclonal human plasma antibodies. *Cell Host & Microbe* **2021**, *29*, 463–476.

(35) Health England, P. SARS-CoV-2 variants of concern and variants under investigation.

(36) Cheng, M. H.; Krieger, J. M.; Kaynak, B.; Arditi, M.; Bahar, I. Impact of South African 501.V2 Variant on SARS-CoV-2 Spike Infectivity and Neutralization: A Structure-based Computational Assessment. *bioRxiv* **2021**, 2021.01.10.426143.

(37) Verkhivker, G. M.; Agajanian, S.; Oztas, D. Y.; Gupta, G. Comparative Perturbation-Based Modeling of the SARS-CoV-2 Spike Protein Binding with Host Receptor and Neutralizing Antibodies: Structurally Adaptable Allosteric Communication Hotspots Define Spike Sites Targeted by Global Circulating Mutations. *Biochemistry* **2021**,

(38) Wang, W. B.; Liang, Y.; Jin, Y. Q.; Zhang, J.; Su, J. G.; Li, Q. M. E484K mutation in SARS-CoV-2 RBD enhances binding affinity with hACE2 but reduces interactions

with neutralizing antibodies and nanobodies: Binding free energy calculation studies. *bioRxiv* **2021**, 2021.02.17.431566.

(39) Spinello, A.; Saltalamacchia, A.; Borišek, J.; Magistrato, A. Allosteric Cross-Talk among Spike's Receptor-Binding Domain Mutations of the SARS-CoV-2 South African Variant Triggers an Effective Hijacking of Human Cell Receptor. *The Journal of Physical Chemistry Letters* **2021**, *12*, 5987–5993.

(40) Golcuk, M.; Hacisuleyman, A.; Erman, B.; Yildiz, A.; Gur, M. Binding mechanism of neutralizing Nanobodies targeting SARS-CoV-2 Spike Glycoprotein. *bioRxiv* **2021**, 2021.04.23.441186.

(41) Pavlova, A.; Zhang, Z.; Acharya, A.; Lynch, D. L.; Pang, Y. T.; Mou, Z.; Parks, J. M.; Chipot, C.; Gumbart, J. C. Machine Learning Reveals the Critical Interactions for SARS-CoV-2 Spike Protein Binding to ACE2. *The Journal of Physical Chemistry Letters* **2021**, *12*, 5494–5502.

(42) Mugnai, M. L.; Templeton, C.; Elber, R.; Thirumalai, D. Role of Long-range Allosteric Communication in Determining the Stability and Disassembly of SARS-COV-2 in Complex with ACE2. *bioRxiv* **2020**, 2020.11.30.405340.

(43) Uyar, A.; Dickson, A. Perturbation of ACE2 structural ensembles by SARS-CoV-2 spike protein binding. *bioRxiv* **2021**, 2021.03.02.433608.

(44) Jo, S.; Kim, T.; Iyer, V. G.; Im, W. CHARMM-GUI: A web-based graphical user interface for CHARMM. *Journal of Computational Chemistry* **2008**, *29*, 1859–1865.

(45) Hopkins, C. W.; Le Grand, S.; Walker, R. C.; Roitberg, A. E. Long-Time-Step Molecular Dynamics through Hydrogen Mass Repartitioning. *Journal of Chemical Theory and Computation* **2015**, *11*, 1864–1874.

(46) Humphrey, W.; Dalke, A.; Schulten, K. VMD: Visual molecular dynamics. *Journal of Molecular Graphics* **1996**, *14*, 33–38.

(47) Huang, J.; Mackerell, A. D. CHARMM36 all-atom additive protein force field: Validation based on comparison to NMR data. *Journal of Computational Chemistry* **2013**, *34*, 2135–2145.

(48) Jorgensen, W. L.; Chandrasekhar, J.; Madura, J. D.; Impey, R. W.; Klein, M. L. Comparison of simple potential functions for simulating liquid water. *The Journal of Chemical Physics* **1983**, *79*, 926–935.

(49) Phillips, J. C.; Braun, R.; Wang, W.; Gumbart, J.; Tajkhorshid, E.; Villa, E.; Chipot, C.; Skeel, R. D.; Kalé, L.; Schulten, K. Scalable molecular dynamics with NAMD. *Journal of Computational Chemistry* **2005**, *26*, 1781–1802.

(50) Abraham, M. J.; Murtola, T.; Schulz, R.; Páll, S.; Smith, J. C.; Hess, B.; Lindah, E. Gromacs: High performance molecular simulations through multi-level parallelism from laptops to supercomputers. *SoftwareX* **2015**, *1-2*, 19–25.

(51) Scherer, M. K.; Trendelkamp-Schroer, B.; Paul, F.; Pérez-Hernández, G.; Hoffmann, M.; Plattner, N.; Wehmeyer, C.; Prinz, J.-H.; Noé, F. PyEMMA 2: A Software Package for Estimation, Validation, and Analysis of Markov Models. *Journal of Chemical Theory and Computation* **2015**, *11*, 5525–5542.

(52) NAMD Energy Plugin, Version 1.4. *https://www.ks.uiuc.edu/Research/vmd/plugins/namdenergy/*

(53) Kraskov, A.; Stögbauer, H.; Grassberger, P. Estimating mutual information. *Physical Review E* **2004**, *69*, 066138.

(54) Lange, O. F.; Grubmüller, H. Generalized correlation for biomolecular dynamics. *Proteins: Structure, Function, and Bioinformatics* **2006**, *62*, 1053–1061.

(55) Bowerman, S.; Wereszczynski, J. *Methods in Enzymology*; Academic Press Inc., 2016; Vol. 578; pp 429–447.

(56) Rivalta, I.; Sultan, M. M.; Lee, N.-S.; Manley, G. A.; Loria, J. P.; Batista, V. S. Allosteric pathways in imidazole glycerol phosphate synthase. *Proceedings of the National Academy of Sciences* **2012**, *109*, E1428–E1436.

(57) Negre, C. F. A.; Morzan, U. N.; Hendrickson, H. P.; Pal, R.; Lisi, G. P.; Loria, J. P.; Rivalta, I.; Ho, J.; Batista, V. S. Eigenvector centrality for characterization of protein allosteric pathways. *Proceedings of the National Academy of Sciences* **2018**, *115*, E12201–E12208.

(58) Ray, D.; Le, L.; Andricioaei, I. Distant Residues Modulate Conformational Opening in SARS-CoV-2 Spike Protein. *bioRxiv* **2021**, 2020.12.07.415596.

(59) Grant, B. J.; Rodrigues, A. P. C.; ElSawy, K. M.; McCammon, J. A.; Caves, L. S. D. Bio3d: an R package for the comparative analysis of protein structures. *Bioinformatics* **2006**, *22*, 2695–2696.

(60) Park, S.; Khalili-Araghi, F.; Tajkhorshid, E.; Schulten, K. Free energy calculation from steered molecular dynamics simulations using Jarzynski's equality. *The Journal of Chemical Physics* **2003**, *119*, 3559–3566.

(61) Onufriev, A.; Bashford, D.; Case, D. A. Exploring protein native states and large-scale conformational changes with a modified generalized born model. *Proteins: Structure, Function, and Bioinformatics* **2004**, *55*, 383–394.

(62) Fiorin, G.; Klein, M. L.; Hénin, J. Using collective variables to drive molecular dynamics simulations. *Molecular Physics* **2013**, *111*, 3345–3362.

Supporting information for "Mutations in SARS-CoV-2 Variants Modulate the Microscopic Dynamics of Neutralizing Antibodies"

Dhiman Ray,[†] Riley Nicolas Quijano,[†] and Ioan Andricioaei[*,‡,‡]

†*Department of Chemistry, University of California Irvine, Irvine CA 92697*

‡*Department of Physics and Astronomy, University of California Irvine, Irvine CA 92697*

E-mail: andricio@uci.edu

Table 1: A list of simulations performed in the current study

System	Variant	Strain	RBD Mutations	Unbiased MD	SMD
RBD only	WT	WT	-	0.3μs×1	-
	alpha	B.1.1.7	N501Y	0.3μs×1	-
	beta	B1.351	N501Y,K417N,E484K	0.3μs×1	-
	kappa	B.1.617	L452R,E484Q	0.3μs×1	-
RBD + B38 Ab	WT	WT	-	0.5μs×1	10ns×5
	alpha	B.1.1.7	N501Y	0.5μs×1	10ns×5
	beta	B1.351	N501Y,K417N,E484K	0.5μs×1	10ns×5
	kappa	B.1.617	L452R,E484Q	0.5μs×1	10ns×5
RBD + BD23 Ab	WT	WT	-	0.5μs×1	10ns×5
	alpha	B.1.1.7	N501Y	0.5μs×1	10ns×5
	beta	B1.351	N501Y,K417N,E484K	0.5μs×1	10ns×5
	kappa	B.1.617	L452R,E484Q	0.5μs×1	10ns×5

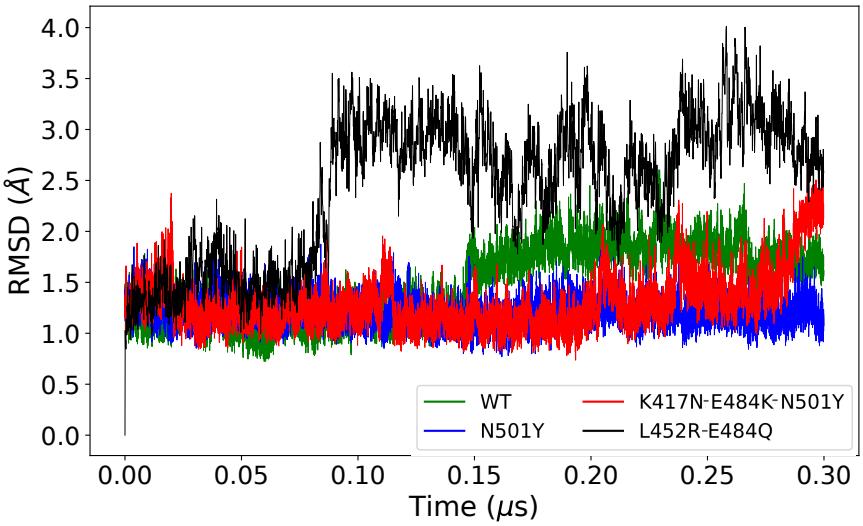

Figure S1: Root mean squared deviations of the bare RBD systems (WT and all mutants) from the long unbiased MD simulation.

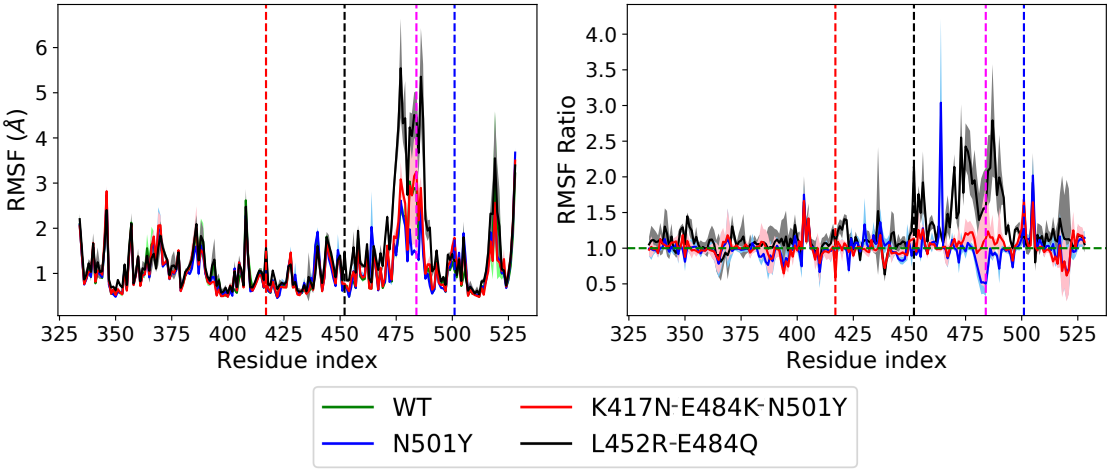

Figure S2: The root mean squared fluctuations (RMSF) of all residues of the bare RBD systems (WT and mutants) and the residue wise RMSF ratio for the three mutant systems.

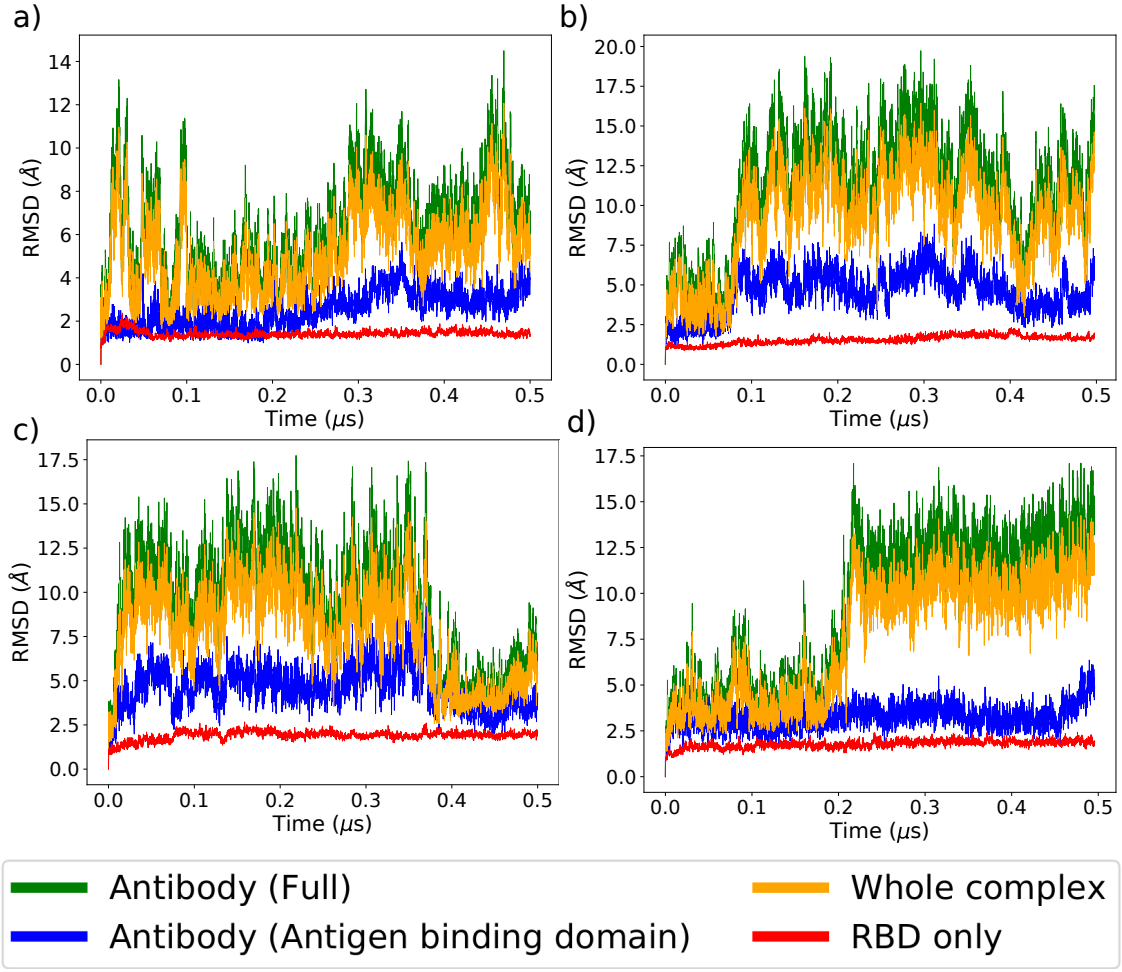

Figure S3: RMSD of different domains of the B38 Fab complex with (a) WT, (b) N501Y mutant, (c) K417N-E484K-N501Y mutant, and (d) L452R-E484Q mutant forms of RBD from the long unbiased MD simulation.

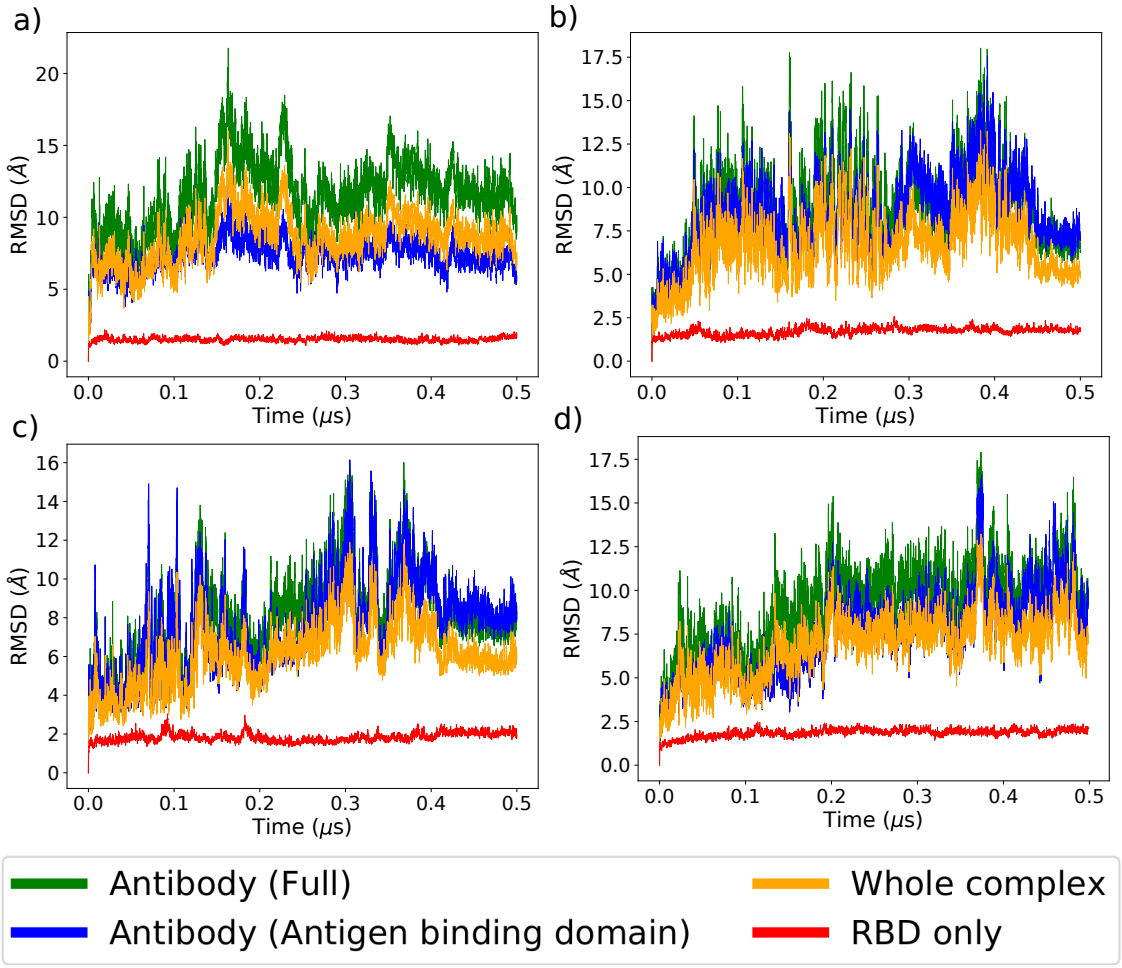

Figure S4: RMSD of different domains of the BD23 Fab complex with (a) WT, (b) N501Y mutant, (c) K417N-E484K-N501Y mutant, and (d) L452R-E484Q mutant forms of RBD from the long unbiased MD simulation.

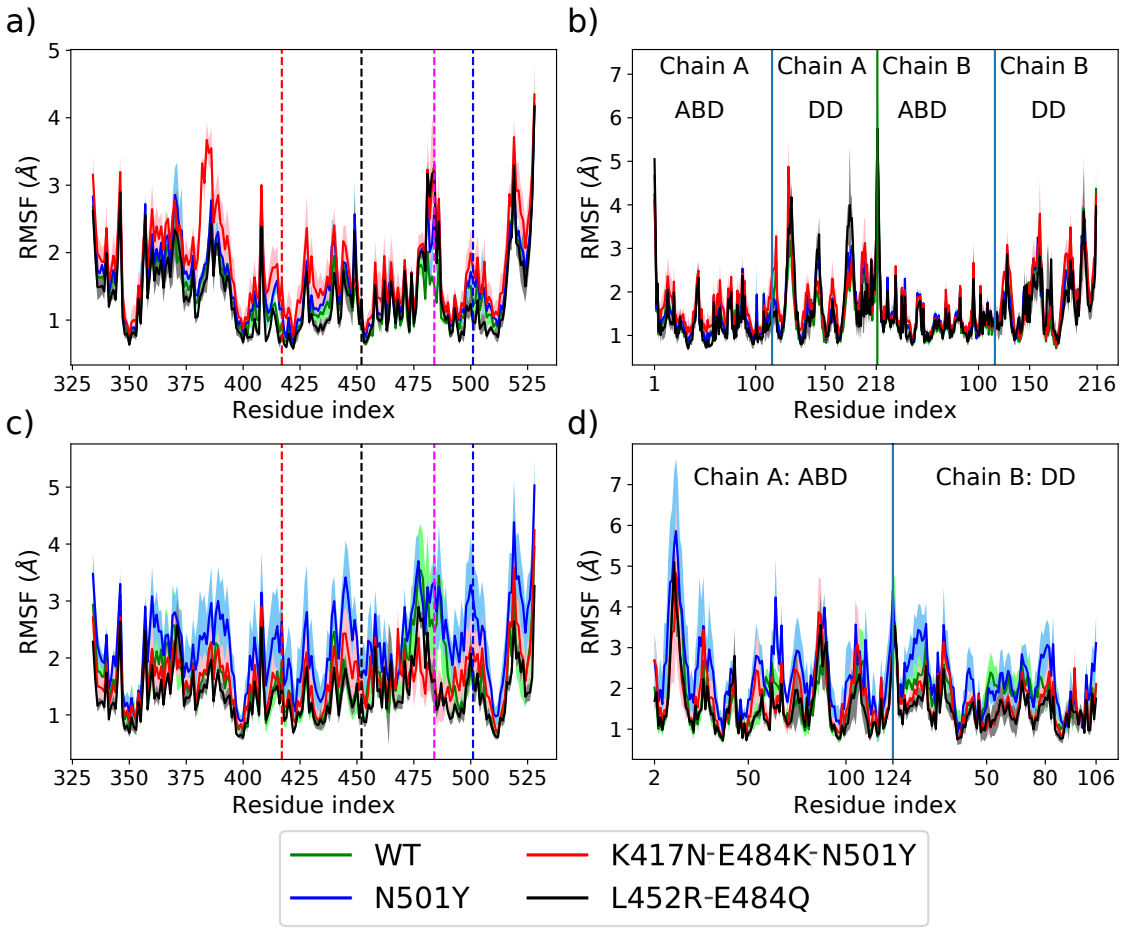

Figure S5: Residue-wise RMSF of all the RBD-antibody complexes: (a) RBD and (b) the antibody part of the RBD-B38 Fab complex and the (c) RBD and (d) the antibody part of the RBD-BD23 Fab complex, for the WT and three mutants. In (a) and (c) the location of mutated residues are marked in dashed line with the following color code; red: 417, black: 452, pink: 484 and blue: 501.

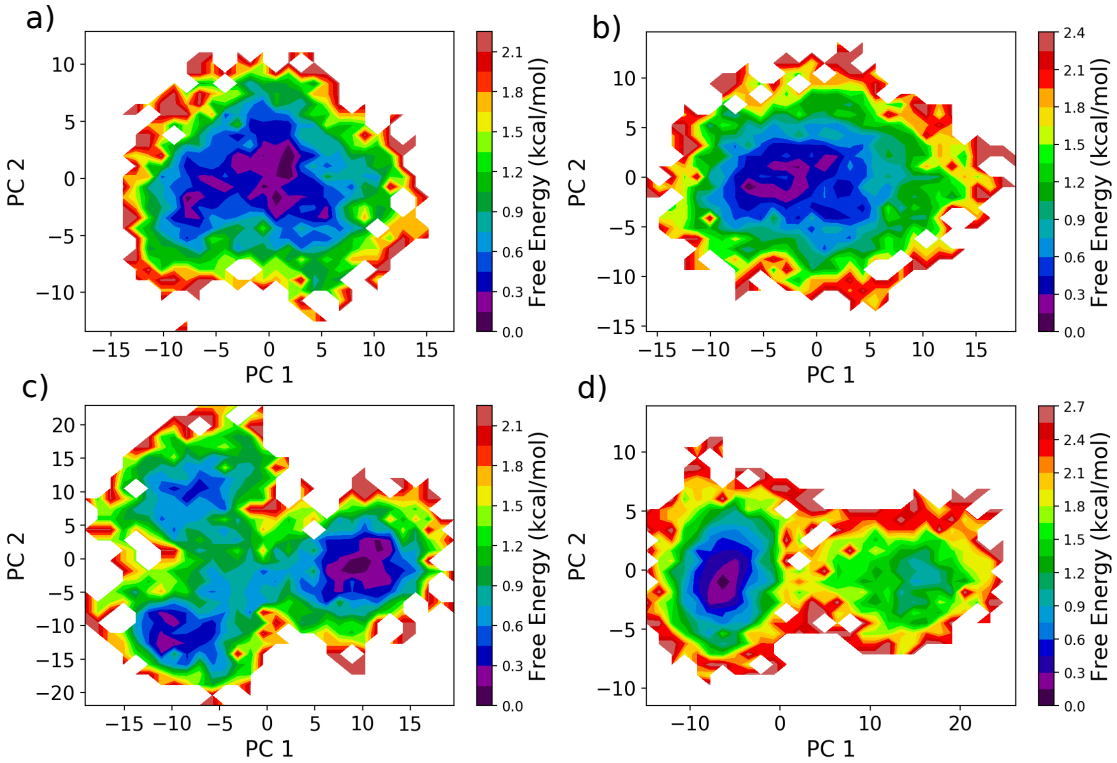

Figure S6: The free energy landscape of the RBD-B38 Fab complexes projected along the first two principal components, for (a) the WT, (b) N501Y mutant, (c)K417N-E484K-N501Y mutant, and (d) L452R-E484Q mutant forms.

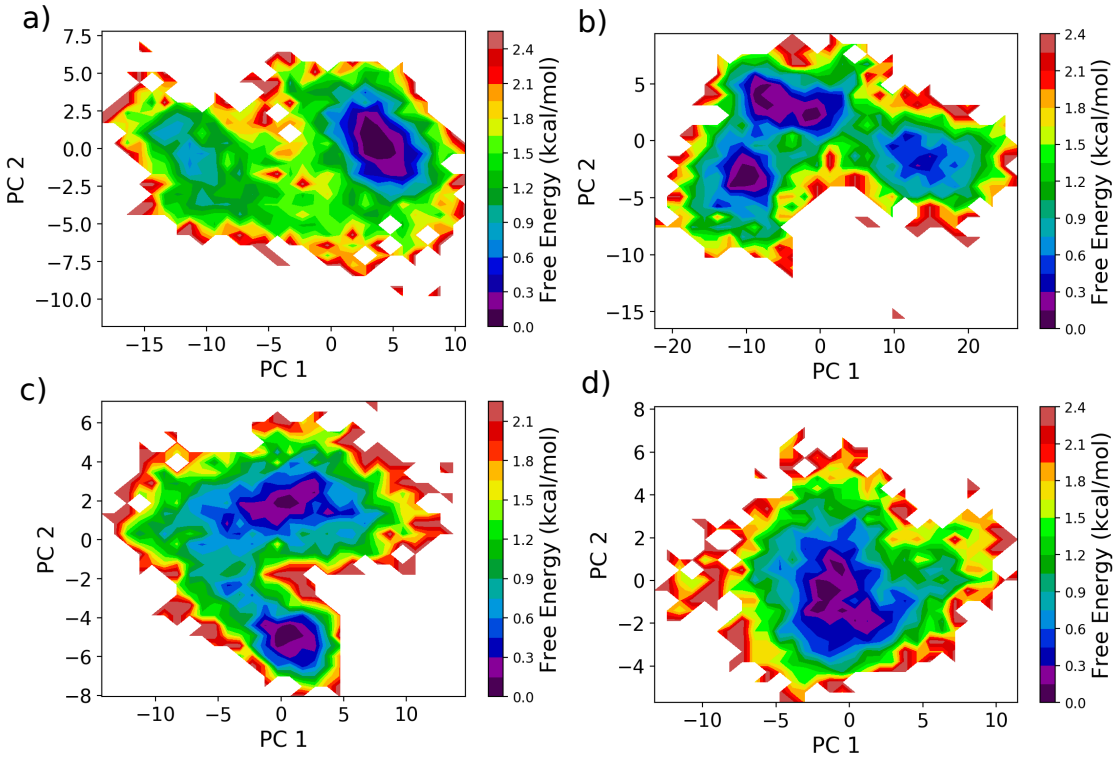

Figure S7: The free energy landscape of the RBD-BD23 Fab complexes projected along the first two principal components, for (a) the WT, (b) N501Y mutant, (c)K417N-E484K-N501Y mutant, and (d) L452R-E484Q mutant forms.

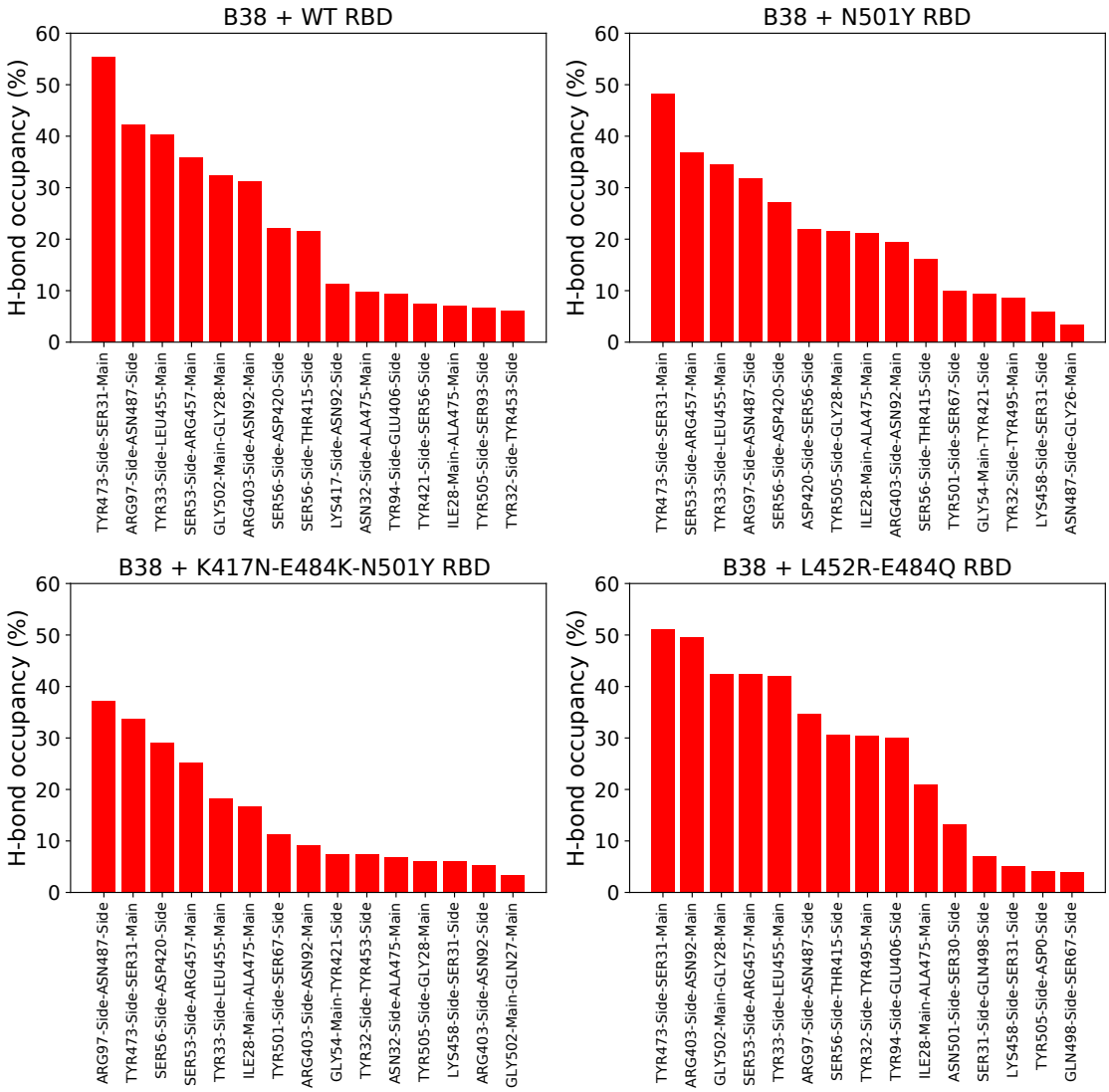

Figure S8: The occupancy of the most prevalent hydrogen bonds between the different variants of the spike RBD and the B38 antibody, sampled from long unbiased simulation.

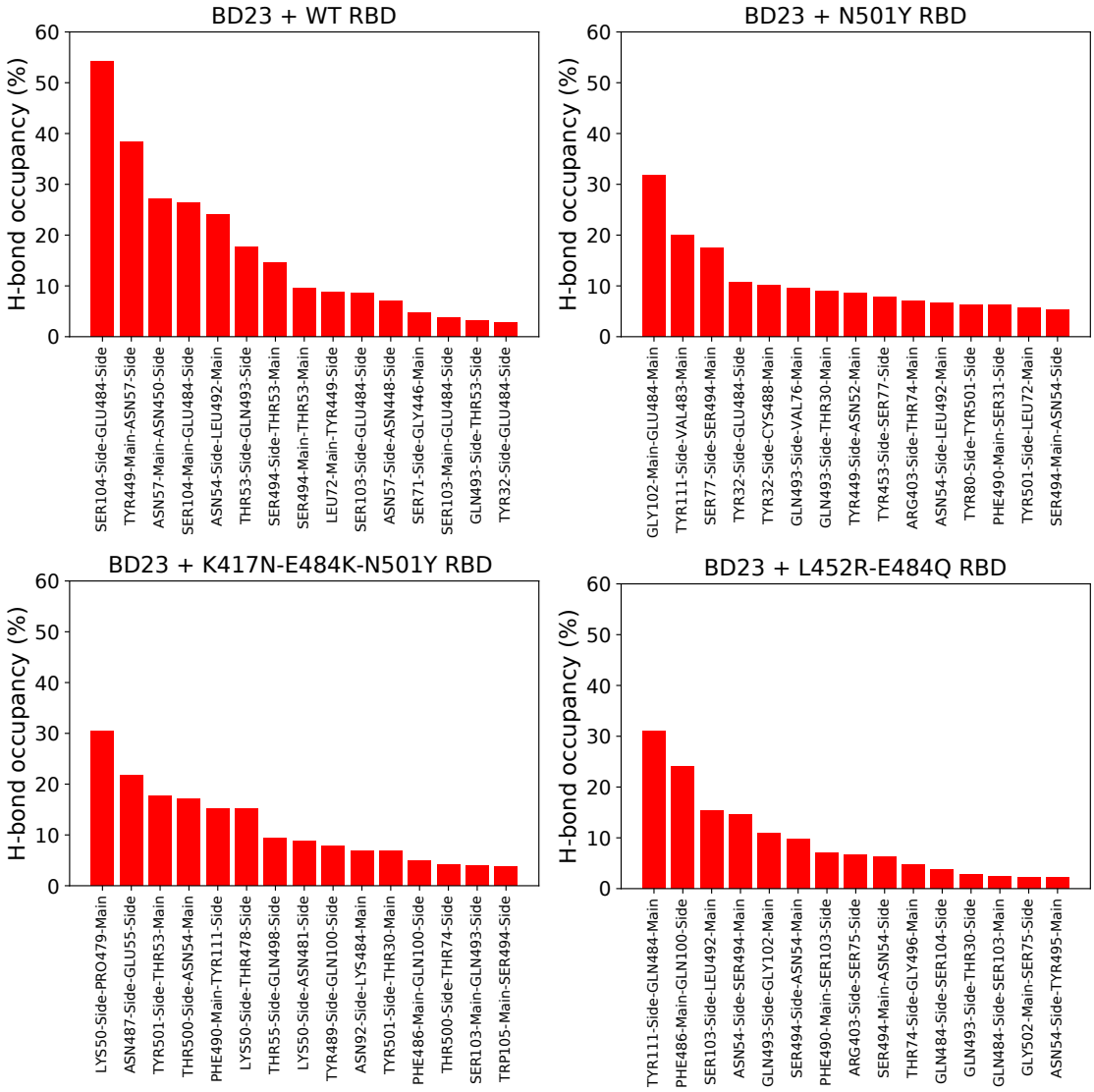

Figure S9: The occupancy of the most prevalent hydrogen bonds between the different variants of the spike RBD and the BD23 antibody, sampled from long unbiased simulation.

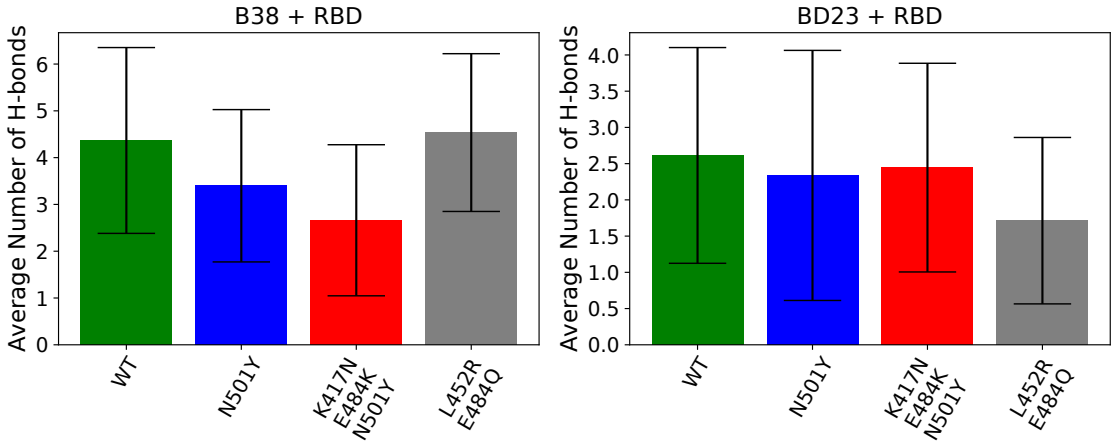

Figure S10: The average number of hydrogen bonds between different variants of the spike RBD and the two antibodies.

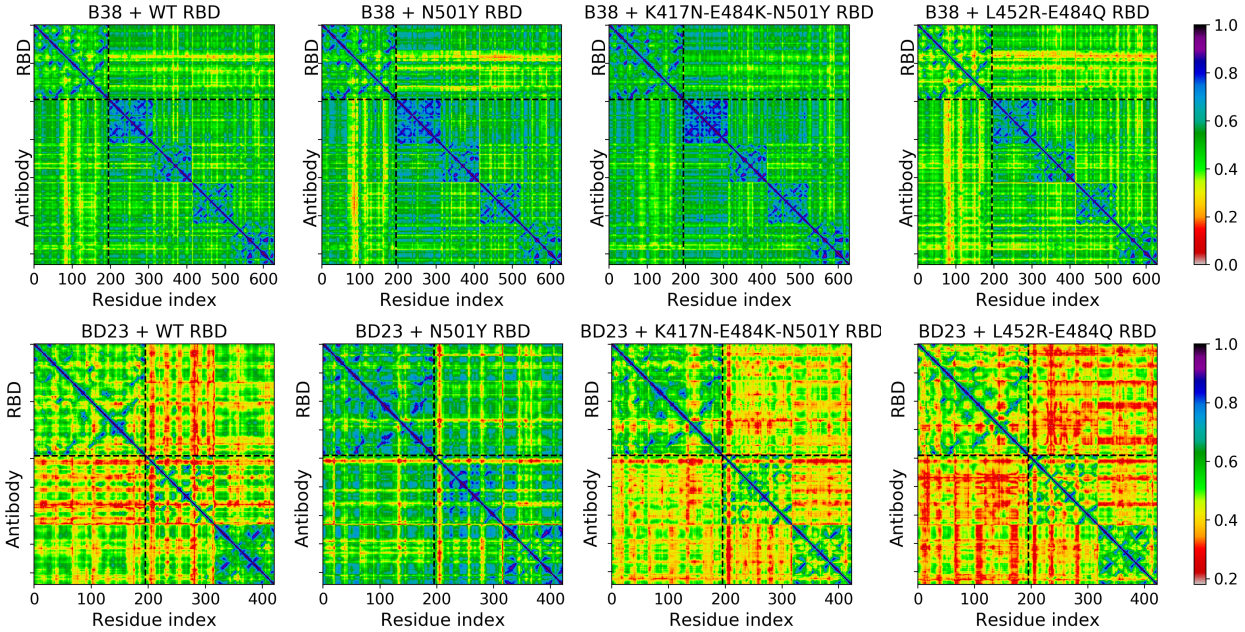

Figure S11: Linear mutual information based cross-correlation between all residue pairs in the RBD-antibody complexes for both the antibodies and all four variants of the RBD.

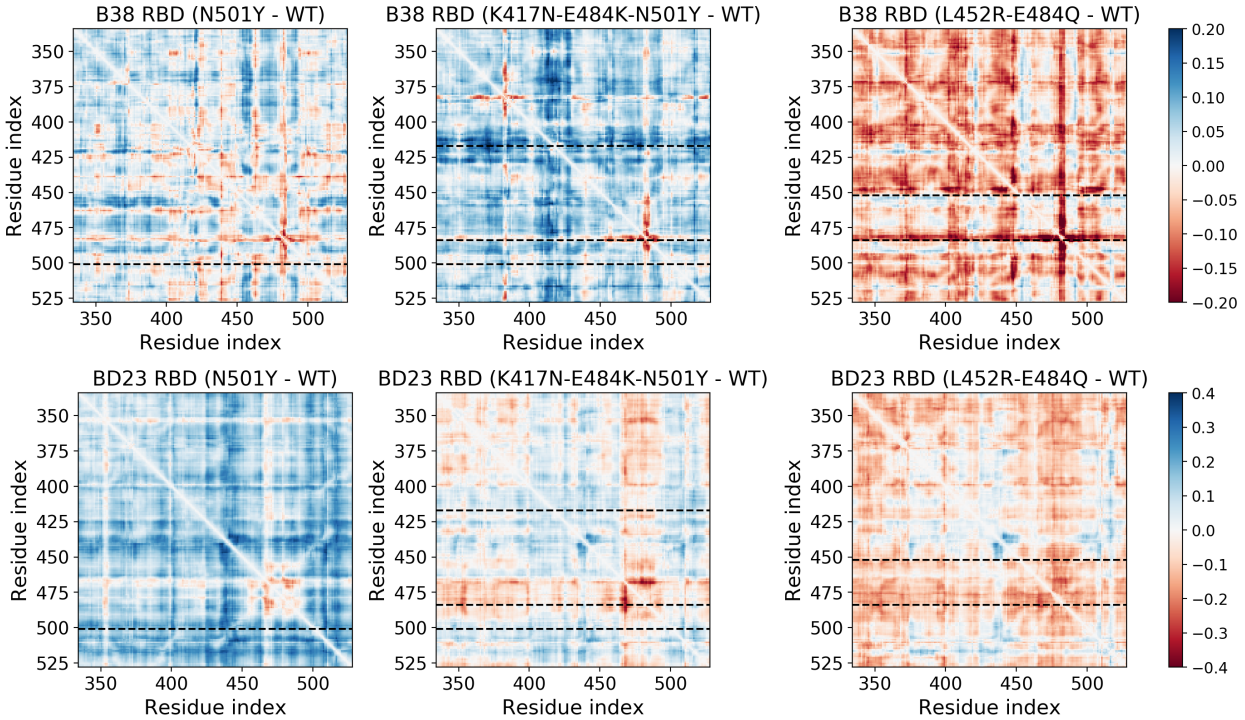

Figure S12: The change in the linear mutual information based cross-correlation between all residue pairs in only the RBD region for different variants and for two antibody systems. The WT-RBD system is considered as reference.

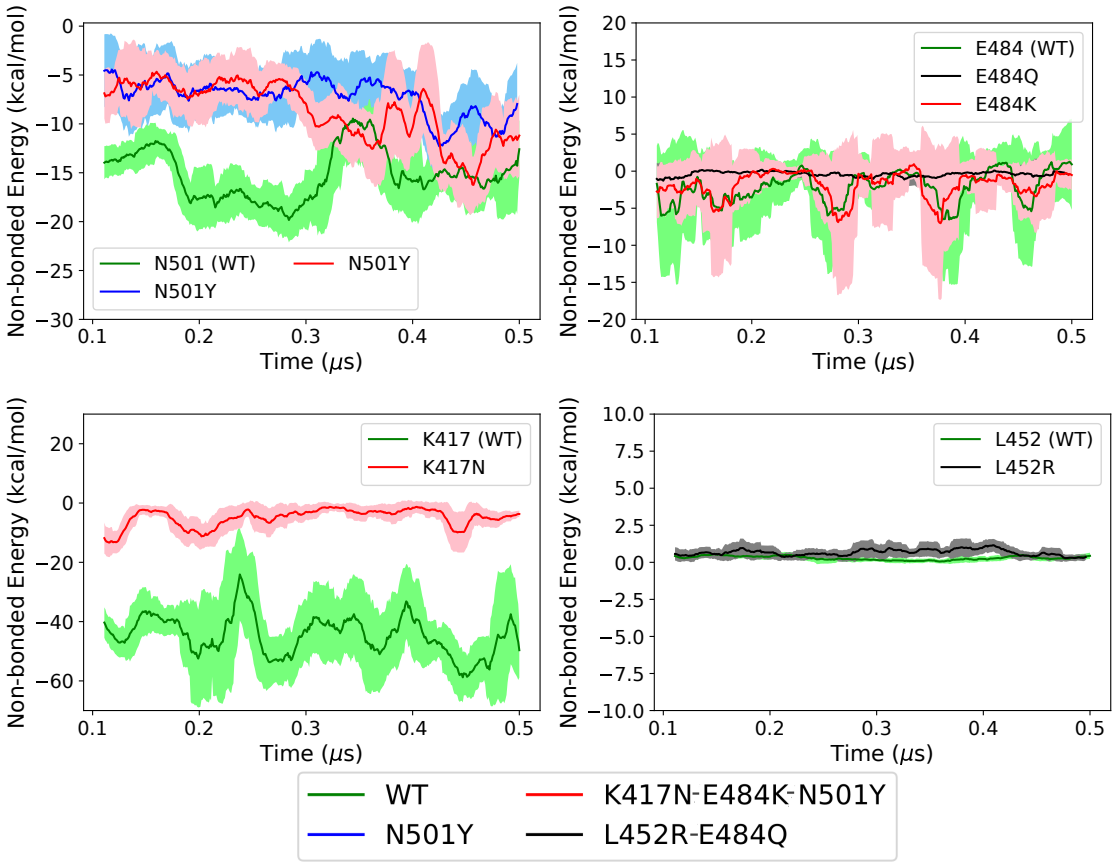

Figure S13: The non-bonded interaction energy between the B38 antibody and each individual RBD residue, mutated in the different variants. The error bars are running average over 20 ns.

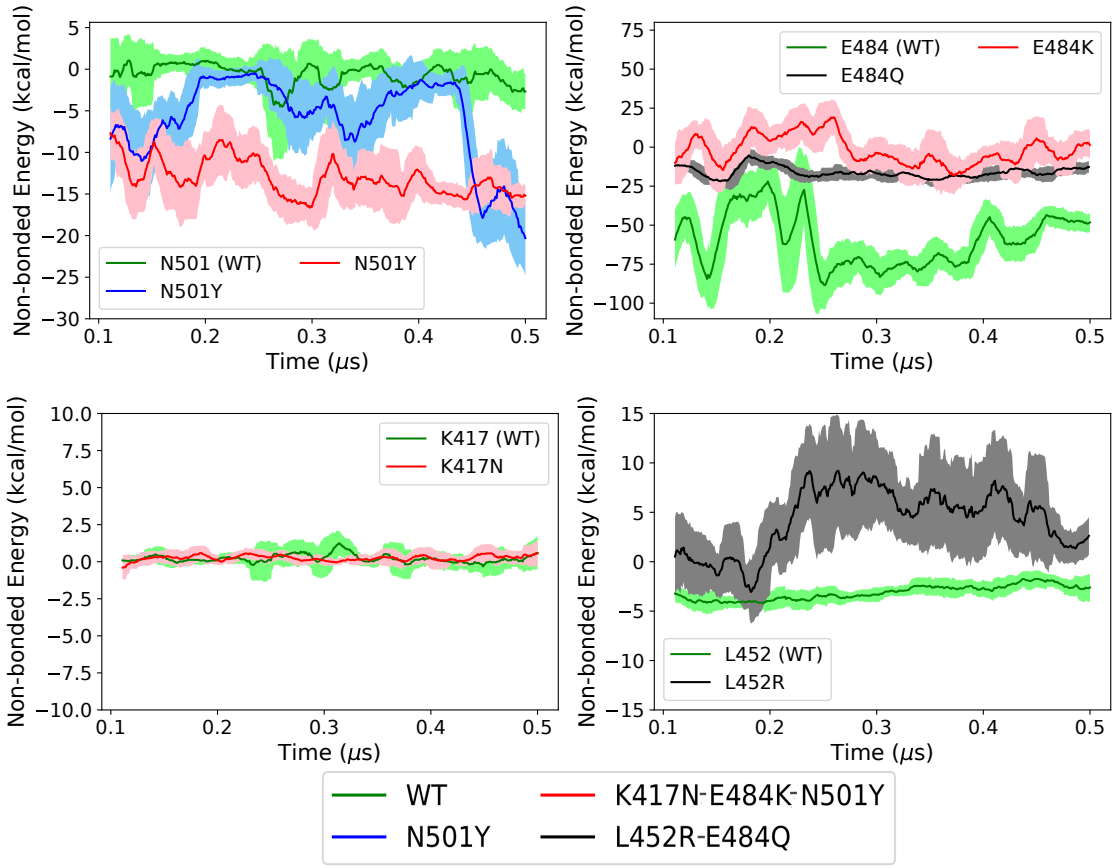

Figure S14: The non-bonded interaction energy between the BD23 antibody and each individual RBD residue, mutated in the different variants. The error bars are running average over 20 ns.

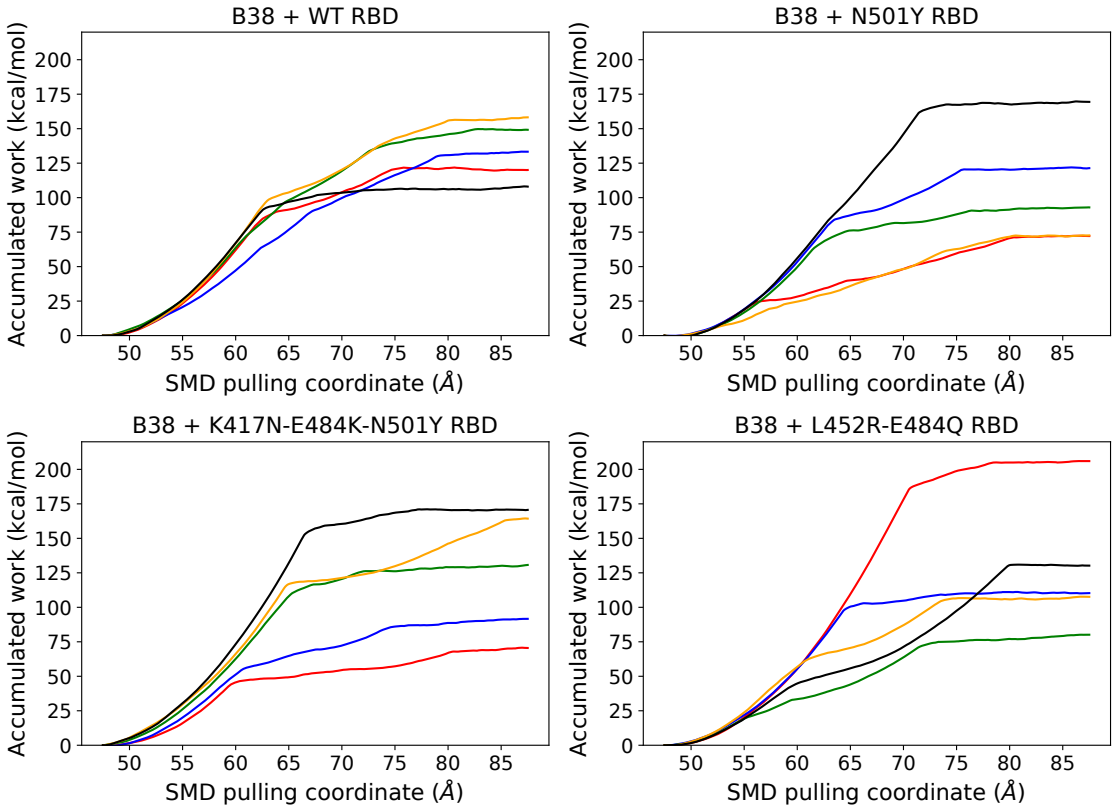

Figure S15: The work required to pull the B38 antibody along the center of mass distance between the RBD and antibody in the SMD simulation. The starting structures for each SMD simulation is sampled from long unbiased simulation after 300, 350, 400, 450 and 500 ns. The color scheme for these five SMD trajectories are as follows: red: 300 ns, blue: 350 ns, green: 400 ns, orange: 450 ns, and black: 500 ns.

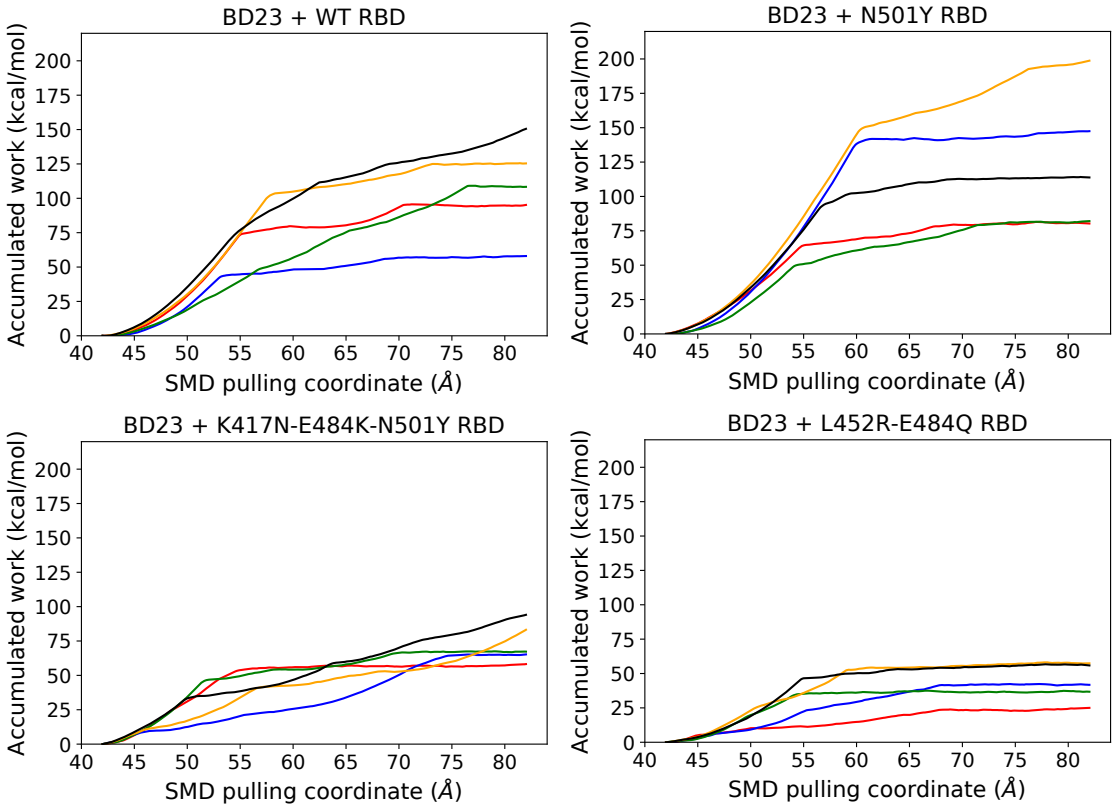

Figure S16: Identical to Figure S15, except for the antibody BD23 Fab.

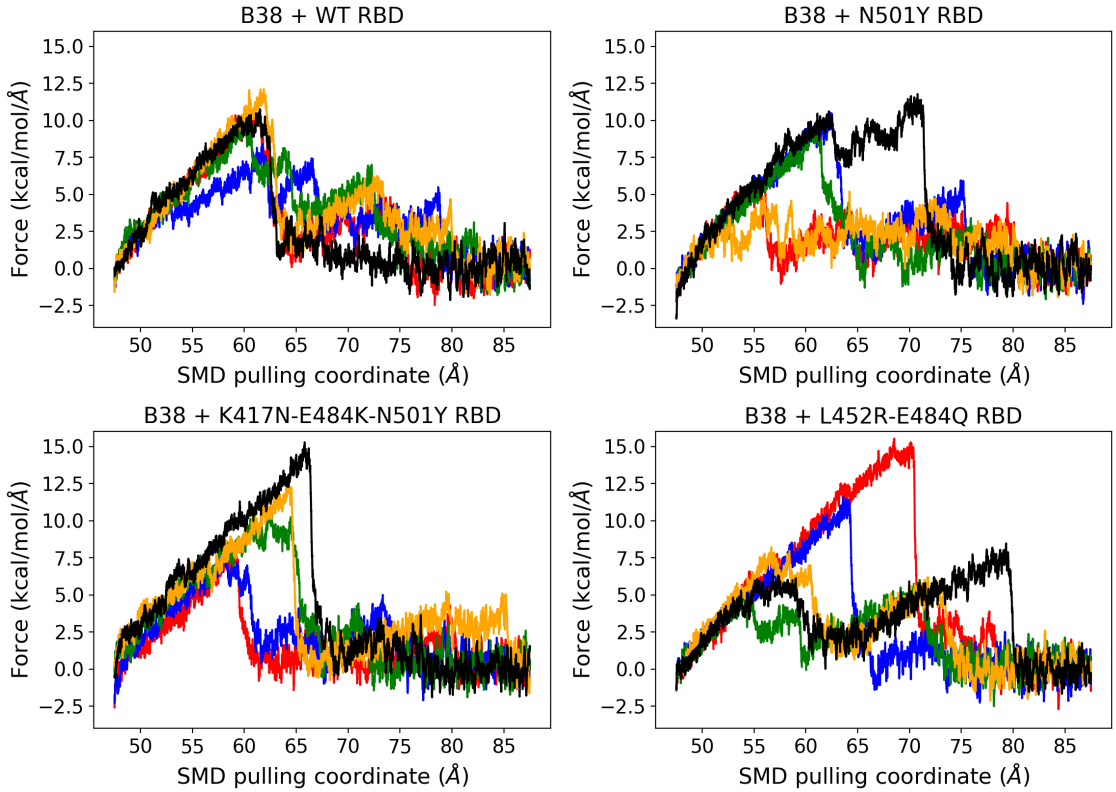

Figure S17: The pulling force required to move the B38 antibody away from the WT and the mutant RBDs along the center of mass distance between RBD and Ab. The color scheme is same as Fig. S15

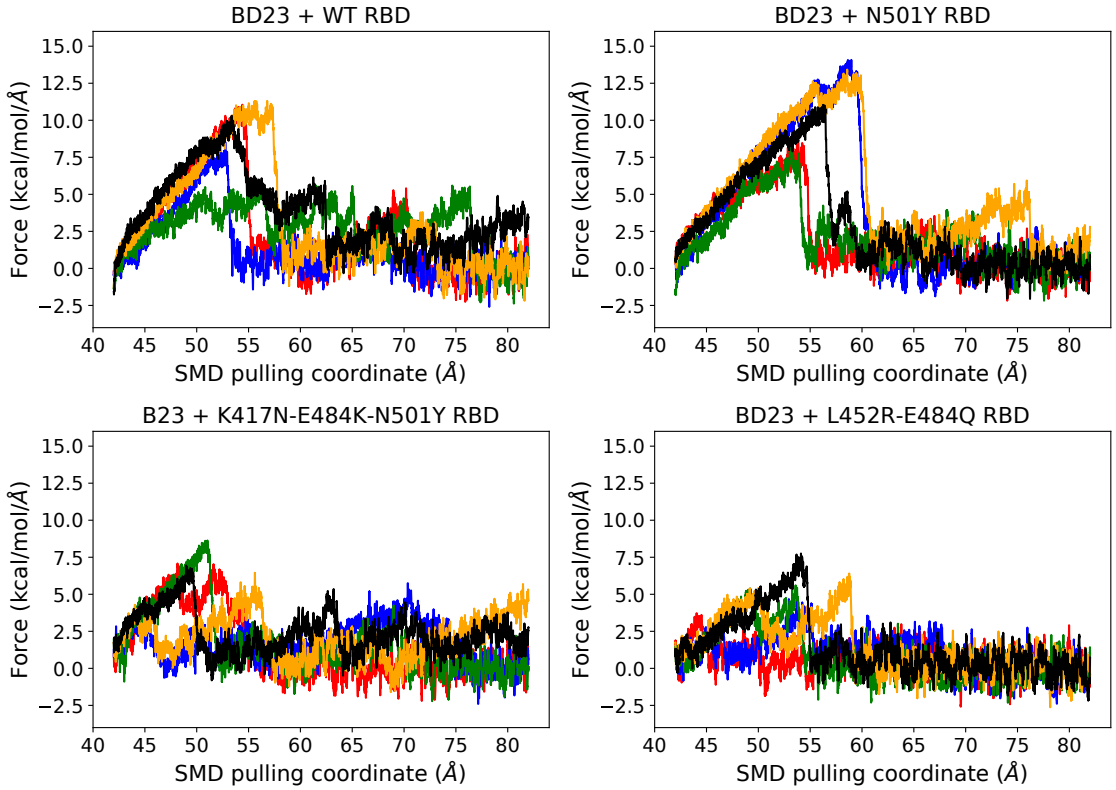

Figure S18: Identical to Figure S17, except for the antibody BD23 Fab.

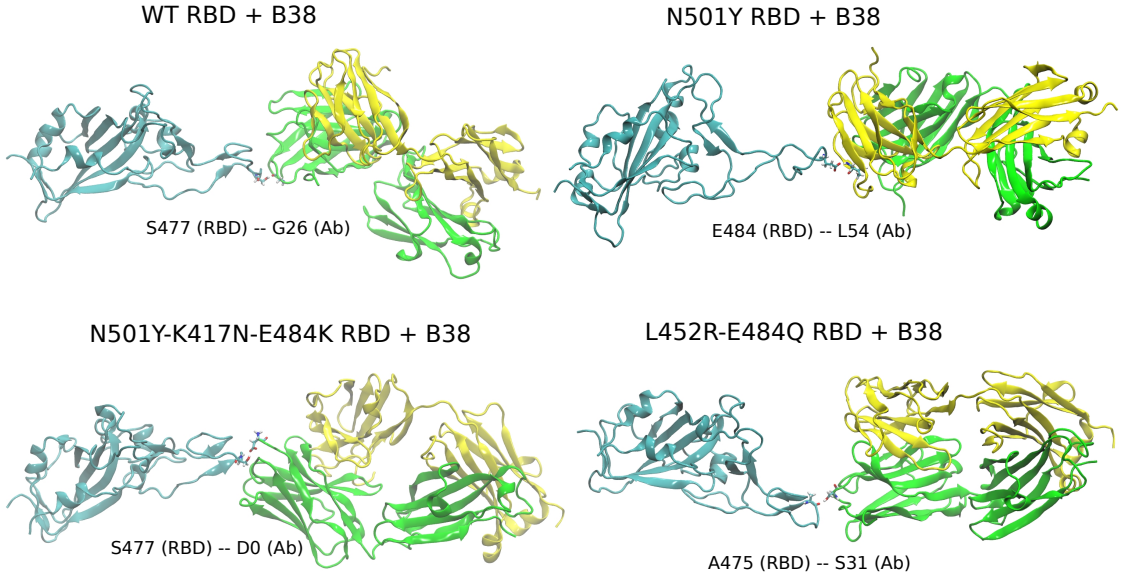

Figure S19: The intermediate structures of the B38 dissociation from the RBD of different variants, sampled from the lowest work SMD trajectory for each respective system. The figure depicts the last intact hydrogen bond between RBD and antibody during the dissociation process.

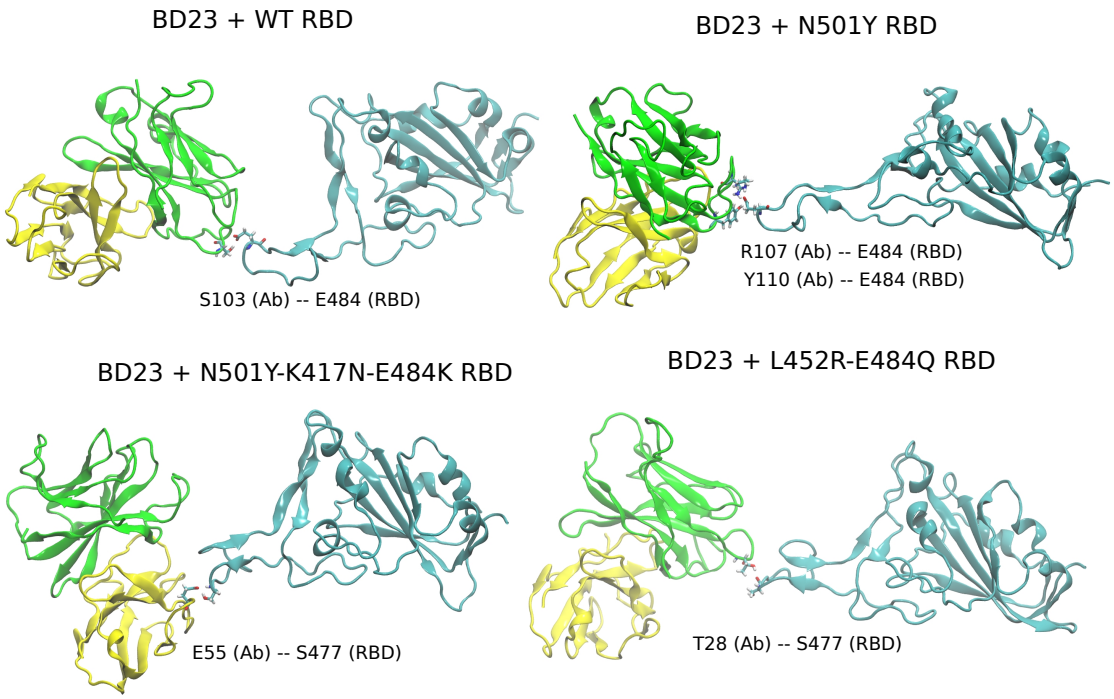

Figure S20: Identical to Figure S19, except for the antibody BD23 Fab.